

Research Articles: Behavioral/Cognitive

Increased hippocampal excitability and altered learning dynamics mediate cognitive mapping deficits in human aging

<https://doi.org/10.1523/JNEUROSCI.0528-20.2021>

Cite as: J. Neurosci 2021; 10.1523/JNEUROSCI.0528-20.2021

Received: 5 March 2020

Revised: 15 January 2021

Accepted: 20 January 2021

This Early Release article has been peer-reviewed and accepted, but has not been through the composition and copyediting processes. The final version may differ slightly in style or formatting and will contain links to any extended data.

Alerts: Sign up at www.jneurosci.org/alerts to receive customized email alerts when the fully formatted version of this article is published.

Copyright © 2021 Diersch et al.

This is an open-access article distributed under the terms of the Creative Commons Attribution 4.0 International license, which permits unrestricted use, distribution and reproduction in any medium provided that the original work is properly attributed.

30 **ABSTRACT**

31 Learning the spatial layout of a novel environment is associated with dynamic activity changes in the
32 hippocampus and in medial parietal areas. With advancing age, the ability to learn spatial environments
33 deteriorates substantially but the underlying neural mechanisms are not well understood. Here, we report
34 findings from a behavioral and a fMRI experiment where healthy human older and younger adults of either sex
35 performed a spatial learning task in a photorealistic virtual environment. We modeled individual learning
36 states using a Bayesian state-space model and found that activity in retrosplenial cortex/parieto-occipital
37 sulcus and anterior hippocampus did not change systematically as a function learning in older compared to
38 younger adults across repeated episodes in the environment. Moreover, effective connectivity analyses
39 revealed that the age-related learning deficits were linked to an increase in hippocampal excitability.
40 Together, these results provide novel insights into how human aging affects computations in the brain's
41 navigation system, highlighting the critical role of the hippocampus.

42 **SIGNIFICANCE STATEMENT**

43 Key structures of the brain's navigation circuit are particularly vulnerable to the deleterious consequences of
44 aging, and declines in spatial navigation are among the earliest indicators for a
45 progression from healthy aging to neurodegenerative diseases. Our study is among the first to
46 provide a mechanistic account about how physiological changes in the aging brain affect the
47 formation of spatial knowledge. We show that neural activity in the aging hippocampus and medial
48 parietal areas is decoupled from individual learning states across repeated episodes in a novel spatial
49 environment. Importantly, we find that increased excitability of the anterior hippocampus might
50 constitute a potential neural mechanism for cognitive mapping deficits in old age.

51 **INTRODUCTION**

52 Exploring our surroundings has always been one of the hallmarks of human identity. To do so, we need to
53 rapidly generate spatial representations and flexibly retrieve them later. With advancing age, however, these
54 abilities deteriorate considerably (Lester et al., 2017). Older adults are slower in learning novel environments
55 and have problems to utilize this information later (Iaria et al., 2009). Moreover, learning landmark locations
56 during exploratory navigation is more difficult for them (Yamamoto and DeGirolamo, 2012), whereas their
57 spatial memory is relatively preserved for familiar environments (Rosenbaum et al., 2012). As a consequence,
58 they may avoid unfamiliar places and become overwhelmed when confronted with changes in their
59 environment.

60 Although core regions of the brain's navigation circuit in the medial temporal lobe are among the first
61 to be affected during the progression from healthy aging to Alzheimer's disease (AD; Braak and Del Tredici,
62 2015), the neural mechanisms for age-related deficits in spatial learning are still poorly understood, even in
63 healthy older adults. Studies in rodents and non-human primates showed that place cells in the CA3 subfield
64 of the hippocampus exhibit higher firing rates in aged animals during navigation, and they fail to encode new
65 information when rats encounter novel environments (Wilson et al., 2005; Thomé et al., 2016). Moreover,
66 firing patterns of aged CA1 place cells are often unstable across repeated visits to the same environment
67 (Barnes et al., 1997). In humans, in contrast, there is evidence for an age-related hypoactivation in the
68 hippocampus and in medial parietal areas during spatial navigation (Moffat et al., 2006; Konishi et al., 2013).

69 However, whether activity changes in the aging brain are indicative of a compensatory mechanism or
70 a correlate of aberrant processing is a long-standing issue in cognitive neuroscience research on aging (Grady,
71 2012; Morcom and Henson, 2018). Evidence from studies investigating age-related impairments in separating
72 sensory input from mnemonic representations (i.e., pattern separation) suggests that hyperactivity in the
73 dentate gyrus and CA3 may underlie memory deficits in healthy aging (Yassa et al., 2011; Reagh et al., 2018).
74 Hippocampal hyperactivity has been further linked to preclinical markers for AD (Leal et al., 2017).

75 Age-related differences in neural activity may further depend on the point in time when activity is
76 measured during task performance. Studies in younger adults showed that the engagement of the
77 retrosplenial cortex (RSC) and the parieto-occipital sulcus (POS) together with the hippocampus changes over
78 the course of learning (Wolbers and Büchel, 2005; Auger et al., 2015; Brodt et al., 2016; Patai et al., 2019). For
79 example, Wolbers and Büchel (2005) showed that activity in the RSC/POS tracked the learning of relative
80 landmark locations during spatial navigation and increased across learning sessions, whereas hippocampal
81 activity reflected the amount of learning in a given session and decreased over time. Given the time course of
82 its involvement during spatial learning, the RSC has been implicated in the retrieval of hippocampal-
83 dependent memories. It receives inputs from CA1 and the subiculum (Kobayashi and Amaral, 2003; Bzdok et
84 al., 2015) and is known to be involved in the integration of different spatial reference frames as well as in
85 updating spatial representations (Epstein, 2008; Miller et al., 2014). The hippocampus, in turn, particularly its
86 anterior portion, is known for its role in generating (spatial) representations (Zeidman and Maguire, 2016).
87 Moreover, place-cell like activity in the RSC of mice relies on intact input from the hippocampus to support
88 memory retrieval (Mao et al., 2018).

89 Here, we report findings from two experiments where we 1) characterized age-related
 90 problems in learning a novel environment, and 2) investigated the underlying neural mechanisms using fMRI.
 91 We focused on activity changes in the RSC/POS and the hippocampus and changes in effective connectivity
 92 within and between the two regions. This allowed us to test whether age-related problems in retrieving newly
 93 learnt information during spatial navigation is linked to a malfunctioning of the integration of hippocampal
 94 input within RSC/POS and/or a corrupted hippocampal signal.

95 MATERIAL AND METHODS

96 *Participants*

97 In the behavioral experiment, 17 younger (9 female, mean age: 24.0 ± 1.66 , age range: 21-28) and 17 older
 98 adults took part (8 female, mean age: 66.4 ± 2.69 , age range: 61-72). All of them were right-handed (LQ: 91.9
 99 ± 11.0 ; Oldfield, 1971) and the older adults showed no signs of major cognitive impairment with scores higher
 100 than 23 in the Montreal Cognitive Assessment (MoCA score: 26.9 ± 2.18 ; Nasreddine et al., 2005; Luis et al.,
 101 2009).

102 To determine the required sample size for the fMRI experiment, we ran a power analysis with the
 103 effect size that was obtained in the behavioral experiment for the interaction between age group and learning
 104 blocks ($\eta_p^2 = .188$), using G*Power 3.1 ($\alpha = 0.05$, $1 - \beta = 0.95$, 2 groups, 8 repeated measurements; Faul et al.,
 105 2007). The power analysis further considered the most conservative correction for non-sphericity with
 106 $1/\text{number of measurements} - 1$. This analysis indicated a requirement of 28 participants in total. We decided to
 107 double this number and recruited a total of 64 participants (27 younger adults, 37 older adults). Three
 108 participants (one younger and two older adults) were excluded from further analyses because they were
 109 identified as outliers in the fMRI data quality checks. In addition, one younger and three older adults were
 110 excluded due to problems in following task instructions and/or cybersickness. The final fMRI sample consisted
 111 of 25 younger (13 female, mean age: 23.4 ± 2.18 , age range: 20-26) and 32 older adults (17 female, mean age:
 112 67.3 ± 4.80 , age range: 58-75). They were all right-handed (LQ: 90.4 ± 12.1 ; Oldfield, 1971) and the older adults
 113 did not show signs of major cognitive impairment (MoCA score: 27.6 ± 1.93 , range: 25-31; Nasreddine et al.,
 114 2005).

115 Across experiments, participants had normal or corrected-to-normal vision and none of them
 116 reported a history of psychiatric or neurological diseases or use of medication that might affect task
 117 performance or MRI scanning. In addition, most of the participants already participated in previous
 118 virtual reality (VR) experiments and, hence, were familiar with navigating in these kinds of setups.
 119 Participants provided informed consent and were paid for their participation in accordance with the
 120 local ethics committee.

121 *Virtual Environment*

122 Using 3ds Max (Autodesk, San Rafael, CA, USA), a novel virtual environment (VE) was developed, which
 123 resembled a typical German historic city center consisting of town houses, shops and restaurants. The VE had
 124 a square-like spatial layout with four interconnected 4-way intersections (Figure 1B). At two intersections, a

125 church and a town hall were placed at the end of one of the outgoing streets, whereas a 2D wall displaying a
126 photo texture of a street continuation bordered the remaining street ends. The VE was based on a 3D model of
127 the old city center of Tübingen. All of the participants confirmed to have never visited Tübingen before the
128 time of testing.

129 *Experimental Design and Procedure*

130 Vizard 5.0 (World Viz, Santa Barbara, CA, USA) was used to animate the experiments, which both started with
131 a familiarization phase during which the participants encountered the VE for the first time. Their task during
132 this phase was to collect tokens that were placed at the street ends by actively traveling the VE, using the four
133 arrow keys of a standard computer keyboard. This phase ended once every token was collected, ensuring that
134 they had visited every street at least once. It followed a short practice of the pointing task (8 trials) that was
135 used to measure navigational retrieval in the experiments. In this way, the VE and the task were introduced in
136 a step-wise manner to reduce the impact of different degrees of experience in handling VR setups on
137 task performance (Diersch and Wolbers, 2019).

138 In the behavioral experiment, eight learning blocks were implemented during which eight retrieval
139 phases alternated with seven encoding phases. One navigational retrieval phase consisted of 12 pointing
140 trials. A pointing trial started with participants being passively transported towards one of the intersections
141 starting from one of the four streets leading towards that intersection (Figure 1C, see Video 2 for an
142 example trial). Duration of this travel phase was fixed to 4 s corresponding to 20 virtual meters. The
143 movement stopped at the center of the intersection, a red crosshair appeared in the middle of the screen, and
144 participants were asked to point in the direction of one of the two target landmarks. Pointing was performed
145 by moving the crosshair to the left or right with the arrow keys of the keyboard. Once they believed to have
146 reached the correct position, they confirmed their response by pressing the space bar. Participants were asked
147 to respond as fast and accurately as possible with a time-out of 12 s (corresponding to $1\frac{1}{2}$ 360° turns in the
148 VE). The ITI, showing a fixation cross, was fixed to 1.5 s. Throughout each trial, a picture cue of the target
149 landmark was displayed at the bottom of the screen and the background was obscured by fog to prevent
150 participants from seeing the street ends or target landmarks during pointing. The first seven retrieval phases
151 were followed by an encoding phase during which participants were passively transported around the whole
152 VE (without fog), starting from one of the two target landmarks in clockwise or counterclockwise order,
153 counterbalanced across the experiment (see Video 1 for a short segment of one tour). During encoding,
154 participants were instructed to pay close attention to the spatial layout of the VE and the location of the target
155 landmarks. Passive transportation instead of self-controlled traveling was chosen to ensure that every
156 participant experienced the VE for the same amount of time (duration: 2.88 min per tour). In total, participants
157 performed 96 navigational retrieval trials (4 intersections x 4 directions x 2 target landmarks x 3 repetitions) in
158 a pseudo-randomized order, with the restriction that each intersection/target landmark combination was
159 encountered starting from two of the four possible directions in the first half of the experiment. In the second
160 half of the experiment, divided by a self-timed break, the respective other two directions were used,
161 counterbalanced across participants. This allowed us to examine how experiencing familiar locations from a
162 novel viewpoint affects pointing performance.

163 The fMRI experiment also consisted of eight learning blocks during which eight retrieval phases
164 alternated with seven encoding phases (see Figure 1A for the structure of the fMRI experiment). fMRI
165 scanning started after a familiarization phase outside of the scanner with the same structure as in the
166 behavioral experiment and a short practice phase during structural imaging. One retrieval phase consisted of 8
167 navigational retrieval trials, which were followed by 4 control trials. These control trials also started with a 4 s
168 travel phase towards an intersection, followed by a pointing phase with a crosshair on screen. Here, cued by a
169 corresponding picture, however, participants were instructed to indicate which of the four corner buildings at
170 the intersection had changed its color and was shaded in blue. Their responses in the control task were
171 classified as correct if they were within $\pm 25^\circ$ from the middle of the respective building, approximately
172 corresponding to its outline. Participants moved the crosshair with their index and middle finger for left and
173 right turns and confirmed their responses with their right thumb on a 5-key Lumitouch response box. Again,
174 participants were asked to respond as fast and accurately as possible with a time-out of 12 s. The ITIs had a
175 variable duration of 1-5 s with a mean of 3 s. During retrieval trials, an additional jittered interval of 0.5-1.5 s
176 duration with a mean of 1 s was included after the travel phase/before the crosshair appeared. The structure of
177 the respective encoding tours was the same as in the behavioral experiment (passive traveling with a constant
178 duration of 2.88 min per tour). In total, participants performed 64 navigational retrieval trials (4 intersections x
179 4 directions x 2 target landmarks x 2 repetitions) without the change of directions from the first to the second
180 half of the experiment as in the behavioral experiment. The change in directions was omitted in the fMRI
181 environment to eliminate the potential influence of approaching the intersections from novel viewpoints and
182 to accommodate a reduced number of trials due to the inclusion of the control task. In total, participants
183 performed 32 control trials (4 intersections x 4 directions x 2 repetitions). fMRI scanning consisted of 3 runs
184 that were divided by short breaks with 24 navigational retrieval trials, 12 control trials and 2 encoding tours in
185 the 1st run; 24 navigational retrieval trials, 12 control trials and 3 encoding tours in the 2nd run; and 16
186 navigational retrieval trials, 8 control trials and 2 encoding tours in the 3rd run.

187 --- insert Figure 1 here ---

188 *Bayesian Modeling of Performance Data*

189 In both experiments, subject-specific improvements in navigational performance were estimated by
190 using a Bayesian implementation of a state-space model that is similar to a local level model where
191 the trial outcomes, y , correspond to the observed level, and the state level represents the hidden
192 learning state, μ (Figure 2; Commandeur and Koopman, 2007). The hidden learning state, μ , is
193 following a random walk such that the actual block learning state depends on the learning state from
194 the previous block. Similar state-space models (e.g., Smith et al., 2007) have been used in previous
195 studies to estimate spatial learning (Wolbers and Büchel, 2005; Auger et al., 2015). However, these
196 studies modeled binary data on a trial-by-trial basis, whereas the present study used continuous
197 performance outcomes and focused on estimating spatial learning block-wise instead of trial-wise. To
198 model the learning state block-wise, an intermediate level accounts for the effects of the responses, η ,
199 and shrinks the effects of individual trials within a block towards the block-wise learning state. In this
200 way, the model accounts for the fact that we can only measure behavioral performance but not the

201 effect of learning or navigational improvement, which we expected to change from one encoding
202 phase to the next but not necessarily from trial to trial. Introducing this intermediate level additionally
203 allowed us to incorporate potential missing trials into the response effects, η . In case of missing trials,
204 we estimated $\eta \sim \text{HalfNormal}(\log(\bar{y}_b), 1)$, i.e., using the log of the block mean as location parameter.
205 The model was implemented using the Python interface to Stan, PyStan (Carpenter et al., 2017; Stan
206 Development Team, 2017; see Figure 2-1 for the Stan code). To account for the substantial between-
207 and within subject variability of the data, weakly informative priors were chosen to provide vague
208 guidance for effective sampling. The model was fit for each participant using four chains each with
209 4000 iterations, of which 2000 correspond to the warm up period, totaling 8000 post-warm-up draws.
210 After inference, convergence of the chains was checked by means of the effective sample size and
211 the potential scale reduction factor (Rhat), confirming that our chains mixed well (Gelman and Shirley,
212 2011).

213 --- insert Figure 2 here ---

214 To determine the fit of our model to the data, we performed a posterior predictive check that compares the
215 observed data with simulated data using samples from the posterior distribution. In Figure 2-2A-E, the
216 posterior predictive samples distribution y_{rep} is plotted together with the observed data y for representative
217 individuals from different learning sub-groups in the fMRI experiment (see [Performance Clustering](#) section)
218 showing that our model was adequate to capture the observed data. We further compared our model to an
219 alternative, simpler model where η was removed (i.e., learning was estimated trial-wise instead of block-wise).
220 Using a leave-one-out (LOO) cross-validation (Vehtari et al., 2017), point-wise out-of-sample prediction
221 accuracies were estimated for both models. Comparing them confirmed that the model incorporating the
222 intermediate layer accounting for the response effects, η , provided better fit to the data, as evidenced by
223 positive LOO differences across the whole sample (sample mean = 1209, SE = 242; see Figure 2-2F for a
224 histogram showing the individual LOO difference values).

225 *fMRI Acquisition Parameters*

226 Scanning was performed on a 3T Magnetom Prisma scanner (Siemens Healthcare, Erlangen, Germany) with a
227 20-channel head coil. High-resolution T1-weighted anatomical images were acquired using a MPRAGE
228 sequence (1 mm isotropic resolution; TE = 2,82 ms; TR = 2500 ms; flip angle = 7°). In three functional runs,
229 whole-brain T2*-weighted echo planar images with BOLD contrast were acquired in interleaved bottom-up
230 order (36 slices, 3 mm isotropic resolution; TE = 30 ms; TR = 2000 ms; FoV = 216 mm; 72 x 72 image matrix; flip
231 angle = 90°).

232 *Behavioral and fMRI statistical analyses*

233 Behavioral Analyses

234 Absolute pointing errors (i.e., the deviation of the subject's response from the direction towards the respective
235 target landmark) served as performance measures in both experiments. In the behavioral experiment, we
236 additionally analyzed response times given the change in directions from which the intersections were

237 approached after the first half of the experiment. Where appropriate, analyses of variance (ANOVA) were
238 performed across learning blocks with age-group (younger adults, older adults) as between-subjects' variable.
239 In a control analysis, we checked for potential biases in pointing behavior by applying circular statistics on the
240 signed pointing error data relative to each target landmark for every intersection-direction combination, using
241 the CircStat toolbox in MATLAB (Berens, 2009). In general, a threshold of $p < 0.05$ was considered significant
242 (with correction for the number of tests where applicable).

243 Logistic Regression Model

244 With respect to the behavioral experiment, we were interested in whether two features that characterized
245 age-related differences in performance could be used to predict the age group of our participants. The first
246 feature was the mean amount of learning across all learning blocks, which was calculated based on the
247 differences between individual learning state estimates, derived from the Bayesian state-space model, from
248 two consecutive learning blocks. The estimates from the first learning block after the familiarization phase,
249 during which participants encountered the VE for the first time, were subtracted from chance level
250 performance (90°). In this way, learning related improvements in performance were considered that already
251 took place during the familiarization phase, resulting in pointing errors well below chance level in the first
252 learning block for some participants. The second feature were the changes in response times after the
253 directions changed from which the intersections were approached after the first half of the experiment. These
254 two features were normalized and then fed into a logistic regression model as implemented in Scikit-learn
255 (Pedregosa et al., 2011), with age group as target vector. The regularization parameter was set using a 10-fold
256 nested cross-validation, and the performance of the model was assessed by computing the average area
257 under the curve (AUC) for all folds. In this way, the probability of each individual belonging to the younger or
258 the older age group could be estimated. The resulting probabilities are interpreted in terms of individual
259 performance: those participants with a higher probability of belonging to the younger age group show better
260 performance on the task while a higher probability of being in the older age group relates to poorer
261 navigational performance.

262 Performance Clustering

263 In the analysis of the behavioral data from the fMRI experiment, we assessed whether subjects could be
264 clustered into different learning sub-groups based on their performance. This allowed us to investigate
265 learning-related differences in neural activity at the between-subjects level. For each participant, we created a
266 distribution based on the difference of the latent state distributions of the last and first learning block to
267 capture the overall amount of learning across the experiment. The mean and the standard deviation
268 parameters of this difference distribution were obtained by fitting it to a normal distribution using SciPy
269 (Jones et al., 2001). In this way, the clustering provides a richer source of information to distinguish between
270 different learning sub-groups. For example, taking only the steepness of the curve across learning blocks into
271 account, would not capture differences between very good learners, who learned most of the spatial layout
272 already during familiarization, and very bad learners, with both groups exhibiting flat learning curves.
273 However, they may differ in the uncertainty of their judgments, which is captured by the dispersion of the
274 difference distribution. We used a K-means clustering algorithm as implemented in Scikit-learn (Pedregosa et

275 al., 2011) to identify the centers of a pre-determined number of clusters based on their distances to the data
276 points. To obtain the optimal number of clusters to input into the K-means, we varied the number of possible
277 clusters from 3 to 7 and computed the mean Silhouette Coefficient of all samples per cluster as a measure for
278 the distance between the resulting clusters with values ranging from -1 to 1 (negative values would indicate
279 wrong cluster assignments and values near zero overlapping clusters). We found 5 to be the best choice for the
280 number of learning sub-groups in our sample (respective silhouette scores per tested cluster number: 3: 0.259,
281 4: 0.395, 5: 0.457, 6: 0.429, 7: 0.410). One should note that the results of this data-driven approach to
282 characterize the heterogeneity within the two age groups are specific to our sample and cannot be
283 generalized to the whole population. Different samples of younger and older adults might result in different
284 learning clusters due to different performance levels.

285 fMRI Image Quality Control and Preprocessing

286 The imaging data were first transformed into the Brain Imaging Data Structure (BIDS) format (Gorgolewski et
287 al., 2016). MRIQC (Version 0.9.3; Esteban et al., 2017) was used for checking the quality of the MRI data.
288 MRIQC utilizes tools from different software packages such as FSL or Advanced Normalization Tools (ANTs)
289 to extract image quality metrics (IQMs) and generates visual reports at the individual and group level. This
290 allows the evaluation of different characteristics of the structural and functional MR images, for example,
291 SNR/tSNR, sharpness, and presence of artifacts. Data from one younger adult and two older adults were
292 consequently excluded from further analyses due to strong task-related movement and/or artifacts in several
293 functional runs resulting in low-quality IQMs (e.g., high Ghost-to-Signal ratio, low tSNR). Next, motion
294 correction, slice timing, co-registration, and normalization of the images was performed using fMRIPrep
295 version 1.0.0-rc5 (Esteban et al., 2019) that also draws on different software packages to provide the optimal
296 implementation for different stages of preprocessing. For example, normalization to MNI space was
297 performed using ANTs as a state-of-the-art medical image registration and segmentation toolkit. Finally, the
298 data were smoothed with a 6 mm full-width at half maximum isotropic Gaussian kernel using SPM 12
299 (Wellcome Department of Imaging Neuroscience, London, UK).

300 ROI Definition

301 Based on results from previous studies (Wolbers and Büchel, 2005; Auger et al., 2015; Mao et al., 2018), we
302 defined two regions of interest (ROI), namely, the RSC/POS and the hippocampus. The single ROIs were
303 created based on each participant's T1 structural scan using a semiautomated anatomic reconstruction and
304 labeling procedure as implemented in FreeSurfer v6.0.0 (<http://surfer.nmr.mgh.harvard.edu>; Dale et al., 1999;
305 Fischl et al., 1999). In each hemisphere, labels corresponding to the posterior-ventral part of the cingulate
306 gyrus (area 10) and the parieto-occipital sulcus (area 65) from the Destrieux Atlas and the hippocampus from
307 the subcortical segmentation were extracted (Fischl et al., 2002; Destrieux et al., 2010). The two cortical labels
308 were combined into one RSC/POS ROI. Each ROI was next transformed to MNI space. Hemispheres were
309 combined to one bilateral ROI, thresholded at 0.5, and finally resampled to correspond to the resolution of our
310 functional images. The ROIs were subsequently used in the univariate analysis and for the volumes of interest
311 (VOI) extraction in the effective connectivity analysis. In our definition of the hippocampus ROI, we did not
312 separate between anterior and posterior hippocampus because previous fMRI studies have not reported a

313 clear dissociation along the hippocampal long axis during navigation in healthy aging. Hence, strong a-priori
314 hypotheses about a potential anterior-posterior dissociation seemed unwarranted. Distinctions between
315 anterior or posterior hippocampus in the results presentation refer to the location of the clusters we obtained
316 in our analyses with foci at or anterior to $y = -21$ mm in MNI space being regarded as belonging to the anterior
317 hippocampus (Poppenk et al., 2013).

318 fMRI Univariate Analysis

319 At the single-subject level, a general linear model (GLM) was specified with six regressors of interest for each
320 learning block using a high-pass filter of 100 Hz. For the navigational as well as control retrieval trials, we
321 created regressors for the 4 s travel phase and the pointing phase. For the encoding phases, regressors
322 modeled periods when participants were located within 20 m of the intersection centers (corresponding to the
323 area covered during the retrieval travel phases) as well as outside of these areas. Finally, the time of the
324 button press was modeled as regressor of no interest. All regressors were convolved with the standard
325 canonical hemodynamic response function (HRF) in SPM12. In addition, we included motion parameters, the
326 frame-wise displacement (FD) and aCompCor values (Behzadi et al., 2007), as obtained from fMRIprep
327 preprocessing, in the GLM to control for physiological and movement confounds. In aCompCor, significant
328 principal components are derived from noise regions-of-interest (ROI) in which the time series data are
329 unlikely to be modulated by neural activity. In this way, potential confounding effects of physiological
330 fluctuations that may differ between age groups, such as cardiac pulsations and respiration-induced
331 modulations, are removed from the fMRI time-series.

332 We focused on interaction effects between conditions of interest and age group that are unlikely to
333 be driven by group differences in neurovascular coupling, unlike main effects of age (Rugg and Morcom, 2005;
334 see also Grinband, Steffener, Razlighi, & Stern, 2017). First, we contrasted navigational retrieval trials to
335 control trials to identify general activation patterns in the RSC/POS and the hippocampus during spatial
336 navigation in our complex real-world environment, similar to previous studies investigating age-group
337 differences in spatial navigation (Moffat et al., 2006). We additionally contrasted the travel phases towards
338 the intersections during navigational retrieval trials to the corresponding periods when participants
339 encountered the same areas during the encoding tours. The within-subject effects of learning were assessed
340 by using the normalized differences between learning state estimates (i.e., the outputs from the Bayesian
341 state-space model) from consecutive learning blocks (i.e., amount of learning) as contrast weights over the
342 regressors modeling each travel phase during navigational retrieval per learning block (cf., Wolbers and
343 Büchel, 2005). At the group level, the resulting individual contrast images were entered into two-sample t-
344 tests to assess interactions with age group. Finally, in order to check in which regions activity changes across
345 learning blocks are modulated by the overall learning ability of the individual, we ran an additional analysis in
346 which learning sub-group was added as covariate in the age-group comparisons at the second-level. All
347 contrasts were evaluated at $p < .001$ (uncorrected) and we report activations that survived the FWE-correction
348 for multiple comparisons using a threshold of $p < 0.05$ at the cluster level.

349 In a control analysis, we checked whether learning-related changes within the two ROIs could
350 alternatively be driven by spatial computations in which older and younger adults engage in differently over

351 the course of the experiment. We fitted a separate finite impulse response (FIR) GLM for each participant with
352 the same regressors of interest as in our main GLM described above. The FIR model was set up with eight time
353 bins (2 s duration each, total time window:16 s) as a basis function for the HRF, and FIR time courses (percent
354 signal change per time bin) were extracted within both the hippocampus and the RSC/POS ROIs for the
355 regressors modeling the eight travel phases using MarsBar (Brett et al., 2002). For each participant, we then
356 determined the time bin when the HRF reached its peak, separately for the beginning of learning (first four
357 learning blocks) and the end of learning (last four learning blocks). This approach allowed us to test (i) whether
358 the HRF reached its peak at different time points in the first vs. the second half of the experiment, and (ii)
359 whether this time-to-peak differed between age groups.

360 Effective Connectivity Analysis

361 Effective connectivity within and between the hippocampus and the POS was examined using the parametric
362 empirical Bayesian (PEB) approach in the context of Dynamic Causal Modeling (DCM) as implemented in
363 SPM12 (Friston et al., 2016).

364 GLM and VOI Selection. For the DCM analysis, we created a GLM in which the time-series from our three
365 functional runs were concatenated and added regressors that modeled the mean signal for each run. The
366 amount of learning per learning block was included as parametric modulation of the regressor modeling the
367 travel phase during navigational retrieval trials for each participant. All other regressors were the same as in
368 the first GLM although they were not modeled separately for each learning block. The sanity check of the
369 concatenated GLM revealed that activity in the right anterior hippocampus (27, -9, -15, $Z = 3.97$; 27 voxels)
370 decreased and activity in the left POS (-12, -63, 31, $Z = 3.56$; 42 voxels) increased with the amount of learning
371 in younger adults ($p < 0.05$, FWE-corrected for the respective ROI). No additional activations emerged
372 elsewhere in the brain. When testing for interactions between learning-related activity changes and age group
373 within our ROIs, one cluster within bilateral POS extending to RSC was revealed (15, -66, 44, $Z = 4.23$; 12, -57,
374 4, $Z = 4.21$; -6, -66, 24, $Z = 3.94$; -15, -60, 28, $Z = 3.61$; 369 voxels). Thus, activity in this region increased with
375 learning in younger adults but less so in older adults. The slight differences of these results to the ones from
376 the first GLM are likely related to differences in the design of the two GLMs. Whereas the first GLM was
377 optimized to capture our experimental design as precisely as possible by modeling all regressors of interest
378 separately for each learning block, the concatenated GLM was optimized for the DCM analysis that relies on
379 single-run time-series.

380 BOLD time-series were extracted for each individual using a t-contrast over the regressors modeling
381 the travel phase during navigational retrieval and the amount of learning with a liberal threshold of $p < 0.1$
382 (Note that this threshold was only used for VOI selection, but not in the final DCM statistics). The principal
383 eigenvariate was extracted around the group peak coordinates within the hippocampus and POS as obtained
384 in the univariate analysis of the concatenated GLM and was allowed to vary as an 8 mm sphere centered on
385 the subject-specific maximum constrained by a 24 mm sphere centered on the group maximum and the
386 respective ROI mask. In this way, variation between individuals in the exact location of the effect was
387 considered, given the high heterogeneity in our sample and slightly different peak voxels in the two GLMs.
388 The extractions were corrected using an F-contrast that retained the effects of interest (navigational as well as

389 control retrieval phases, encoding phases, button press) while partitioning out task-unrelated variance caused
 390 by head motion, for example. For participants for which no supra-threshold voxels were identified (three
 391 younger adults and one older adult), the threshold was lowered to $p < 0.5$ to extract BOLD time-series (cf.,
 392 Zeidman et al., 2019b).

393 *First-Level DCM Specification.* We specified a bilinear, one-state DCM for each participant by setting the
 394 regressor modeling the travel phase during navigational retrieval trials as driving input entering the cortical
 395 network via the POS. The amount of learning per learning block was included as modulatory input on the
 396 bidirectional connections between hippocampus and POS. All inputs were mean-centered so that the A-
 397 matrix of the DCM represents the average connectivity across experimental conditions. We used stochastic
 398 DCM that seeks to improve model estimation by modeling random fluctuations and hidden neuronal causes in
 399 the differential equations of the neuronal states (Li et al., 2011; Daunizeau et al., 2012). In this way, the impact
 400 of potential confounding effects of variations in BOLD response caused by age is reduced. Bayesian group
 401 inversion was performed, providing estimates of the connection strength parameters that best explained the
 402 observed data per participant. Critically, within DCM PEB, at each iteration of the within subject inversion, the
 403 individual priors are updated using the group average connection strengths as priors. Inspection of the single
 404 DCMs after inversion confirmed that our full model provided good fit to the observed data with an average of
 405 $44.5 \pm 3.22\%$ variance explained.

406 *Second-Level PEB Model.* Next, we created a second level PEB model over the parameters that included the
 407 group mean and age group as covariates to identify differences between younger and older adults. We further
 408 included learning sub-group and its interaction with age group as covariates in the model. The interaction
 409 term was modelled as the two main effects of age and learning group element-wise multiplied with the main
 410 effects being mean-centered and coded in a way that low/negative values represent younger or better
 411 performing individuals. A search over nested PEB models was performed by using Bayesian model comparison
 412 (BMC) that explores a space of models under the assumption that different combinations of the connections
 413 may exist across participants (Zeidman et al., 2019a). To search over hundreds of nested models incorporating
 414 different combinations of connections and group differences, Bayesian model reduction (BMR) was used that
 415 iteratively prunes parameters from the full model until model-evidence decreases. To reduce dilution of
 416 evidence, we separately checked for group differences in the A-matrix (average connectivity across
 417 experimental conditions) and the B-matrix (within-subject modulatory input of the amount of learning per
 418 block). We further performed a LOO cross-validation to check whether the model parameter that differed
 419 between older and younger adults could be used to predict the participants' age group.

420 *Data Availability*

421 Source data files for the main results figures and tables are stored at <https://osf.io/fjbxu/>. We additionally
 422 provide a key resources table listing all the software packages that were used in the current study. The Stan
 423 code of the Bayesian state-space model can be found in Figure 2-1.

424 **RESULTS**

425 Findings are reported from two separate samples comprising healthy younger and older adults who
 426 performed a spatial learning task either purely behaviorally (17 younger adults and 17 older adults) or in a
 427 combined fMRI-behavioral experiment (25 younger adults and 32 older adults). In both experiments, following
 428 an initial familiarization phase before testing/outside of the scanner, eight learning blocks were implemented
 429 during which eight retrieval phases alternated with seven encoding phases. We used the angular deviation of
 430 the participants' response from the respective target landmark (i.e., absolute pointing errors) to measure
 431 performance improvements across learning blocks. However, performance in these kinds of tasks can be
 432 corrupted by various noise sources and, hence, might not accurately reflect the actual learning state of the
 433 participant. Therefore, subject-specific improvements in navigational performance were estimated by using a
 434 Bayesian implementation of a state-space model that disambiguated learning from random trial-by-trial
 435 fluctuations in performance. We used the outputs of the model in the analysis of the fMRI data to examine
 436 intra- and interindividual differences in learning.

437 ***Behavioral experiment***

438 Lower performance and reduced learning in older adults

439 An ANOVA with learning block (1-8) as repeated measures variable and age-group (younger adults, older
 440 adults) as between-subjects variable on the average absolute pointing errors showed significant main effects
 441 of learning block, $F(7, 224) = 19.5$, $p < .001$, $\eta_p^2 = .379$, and age group, $F(1, 32) = 85.2$, $p < .001$, $\eta_p^2 = .727$. This
 442 was modulated by a significant interaction between the two factors, $F(7, 224) = 7.40$, $p < .001$, $\eta_p^2 = .188$. At the
 443 beginning, both age groups performed around chance level (90°), even though older adults had spent
 444 significantly more time than younger adults ($M_{old} = 534 \text{ s} \pm 161 \text{ s}$; $M_{young} = 218 \text{ s} \pm 41.4 \text{ s}$; $t(16.9) = -7.63$, $p < .001$,
 445 $d = 2.69$) in the initial familiarization phase of the experiment, during which they encountered the VE for the
 446 first time. Over the course of the experiment, however, older adults showed lower performance and less
 447 improvement compared to younger adults (Figure 3A). The change in direction from the first to the second
 448 half of the experiment did not have a major effect on this pattern of results as implied by a non-significant
 449 interaction between learning block and age group when directly comparing the fourth and fifth learning block,
 450 $F(1, 32) = 1.96$, $p = .171$, $\eta_p^2 = .058$. A separate ANOVA within the older age group on pointing performance per
 451 learning block confirmed that older adults generally improved on the task over time as evidenced by a
 452 significant main effect of learning, $F(7, 112) = 2.58$, $p = .017$, $\eta_p^2 = .139$. According to the outputs of the
 453 Bayesian state-space model (Figure 3C, see Figure 3-1A-B for average pointing errors per learning block for
 454 each participant), most of the younger adults learned the spatial layout of the VE very fast, reaching ceiling
 455 performance already after the first few learning blocks. The older adults, in contrast, differed more widely in
 456 their ability to learn.

457 To investigate potential biases in pointing behavior that might differ between the age groups, such as
 458 an increased tendency to point along streets, circular statistics were applied on the signed pointing error data
 459 relative to each target landmark for every intersection-direction combination. From the 32 age-group
 460 comparisons (4 intersections \times 4 directions \times 2 target landmarks), only 7 reached significance as determined by
 461 a Watson-Williams test, all $p \leq .047$. Older adults showed larger deviation from the correct angle than younger

462 adults in 6 of the 7 instances. The direction of the deviations in pointing (e.g., to the left or right relative to the
463 target landmark), however, varied and none of the effects survived when correcting for multiple comparisons.

464 Higher uncertainty when viewpoints are changing in older adults

465 An ANOVA with learning block (1-8) as repeated measures variable and age group (younger adults, older
466 adults) as between-subjects variable on the response time data confirmed significant main effects of learning
467 block, $F(7, 224) = 9.26$, $p < .001$, $\eta_p^2 = .225$, and age group, $F(1, 32) = 10.5$, $p = .003$, $\eta_p^2 = .247$. Compared to
468 older adults, younger adults responded quicker and showed a steeper decline in response times over time as
469 revealed by a significant interaction between learning block and age group, $F(7, 224) = 4.29$, $p = .001$, $\eta_p^2 =$
470 $.118$. Notably, when comparing the fourth and fifth learning blocks, a significant interaction between learning
471 block and age group was obtained, $F(1, 32) = 9.34$, $p = .004$, $\eta_p^2 = .226$. Older but not younger adults showed a
472 substantial increase in response times in the fifth learning block when the intersections were encountered
473 from novel directions (Figure 3B). This result cannot be explained by a confound between pointing
474 performance and required turning at the intersections because the required amount of turning to perform
475 accurately on the task varied from trial to trial, depending on the specific intersection-direction-target
476 landmark combination. Moreover, it was kept constant across experiment halves and participants (average
477 turning direction: 135°). When considering the fourth and fifth block only, the correct turning angle did not
478 differ between blocks, age groups, or varied between age groups as a function of learning block, all $F \leq 3.23$, p
479 $\geq .082$, $\eta_p^2 \leq .092$. Thus, older adults' representations of the spatial layout of the environment seem to be
480 more rigidly tied to the sensory input encountered at the beginning of learning, leading to a temporary
481 uncertainty when viewpoints are suddenly changing.

482 --- insert Figure 3 here ---

483 Performance in older adults is partly influenced by their facing direction

484 Age-related differences in pointing performance depending on the nature of the trials during navigational
485 retrieval (i.e., respective intersection-direction-target landmark combination) were further analyzed by means
486 of an ANOVA on the absolute pointing errors with intersection (I1-I4), direction (D1-D4), and target landmark
487 (town hall, church) as repeated measures variables and age group (younger adults, older adults) as between-
488 subjects variable. A significant interaction between the four factors suggested that the performance of the
489 age groups was modulated by the respective intersection-direction-target landmark combination
490 encountered in the VE during retrieval, $F(9, 288) = 2.05$, $p = .034$, $\eta_p^2 = .060$. Therefore, follow-up ANOVAs
491 were conducted within the two age groups separately. In younger adults, a significant main effect of
492 intersection, $F(3, 48) = 6.18$, $p = .005$, $\eta_p^2 = .279$ (Greenhouse-Geisser corrected), showed that performance was
493 worse when they were located at I4 ($M = 48.6^\circ \pm 21.9^\circ$) as compared to I1 ($M = 25.0^\circ \pm 19.7^\circ$) or I2 ($M = 30.6^\circ \pm$
494 25.7°), all $p \leq .010$ (Bonferroni-corrected). This was modulated by a significant interaction between
495 intersection and target landmark, $F(3, 48) = 11.4$, $p < .001$, $\eta_p^2 = .416$. Pointing errors were smaller in this age
496 group when they pointed towards the town hall ($M = 13.5^\circ \pm 14.5^\circ$) as compared to the church ($M = 36.6^\circ \pm$
497 29.3°) at I1, which was the intersection adjacent to the town hall, and vice versa at I3, which was the
498 intersection adjacent to the church (town hall: $M = 45.5^\circ \pm 35.5^\circ$; church: $M = 25.8^\circ \pm 26.9^\circ$), all $t \geq 3.33$, $p \leq$

499 .004, $d \geq 0.807$. The directions from which the intersections were approached did not have an influence on
 500 performance in this age group, all $F \leq 1.80$, $p \geq .133$, $\eta_p^2 \leq .101$. In older adults, there was also an interaction
 501 between intersection and target landmark, $F(3, 48) = 3.38$, $p = .026$, $\eta_p^2 = .174$. When located at I3, pointing
 502 errors were smaller when the target landmark was the adjacent church ($M = 73.2^\circ \pm 27.4^\circ$) as compared to the
 503 town hall ($M = 94.2^\circ \pm 19.9^\circ$), $t(16) = 2.73$, $p = .015$, $d = 0.662$. The corresponding comparison for I1 did not
 504 reach significance, $t(16) = 1.12$, $p = .281$, $d = 0.271$. In addition, there was a significant interaction between
 505 direction and target landmark, $F(3, 48) = 3.75$, $p = .039$, $\eta_p^2 = .190$ (Greenhouse-Geisser corrected). Post-hoc t-
 506 tests indicated that pointing towards the town hall ($M = 80.3^\circ \pm 18.1^\circ$) tended to be easier as compared to
 507 pointing towards the church ($M = 94.5^\circ \pm 27.1^\circ$) for the older adults when they approached the intersections
 508 from D4 (i.e., facing east), $t(16) = 1.96$, $p = .068$, $d = 0.475$. In contrast, pointing towards the church ($M = 69.9^\circ$
 509 $\pm 19.6^\circ$) tended to be easier than pointing towards the town hall ($M = 87.0^\circ \pm 23.3^\circ$) when they approached the
 510 intersections from D2 (i.e., facing west), $t(16) = 1.99$, $p = .064$, $d = 0.483$. This was modulated by an interaction
 511 between intersection, direction, and target landmark, $F(9, 144) = 2.25$, $p = .022$, $\eta_p^2 = .123$. Separate follow-up
 512 ANOVAs for each intersection with direction (D1-D4) and target landmark (town hall, church) as repeated
 513 measures variables revealed for I2 a main effect of direction, $F(3, 48) = 5.25$, $p = .003$, $\eta_p^2 = .247$, indicating that
 514 pointing generally seemed to be easier from D2 (i.e., facing west; $M = 68.8^\circ \pm 32.7^\circ$) as compared to D1 ($M =$
 515 $94.0^\circ \pm 24.5^\circ$) or D4 ($M = 95.8^\circ \pm 37.1^\circ$), that is, when they were facing towards the dead-ends at this
 516 intersection, all $p \leq .054$ (Bonferroni-corrected). At I3, a main effect of target landmark indicated that pointing
 517 towards the adjacent church ($M = 73.2^\circ \pm 27.4^\circ$) was easier for the older adults than pointing towards the town
 518 hall ($M = 94.2^\circ \pm 20.0^\circ$), $F(3, 48) = 7.47$, $p = .015$, $\eta_p^2 = .318$. This was modulated by an interaction between
 519 direction and target landmark, $F(3, 48) = 4.44$, $p = .008$, $\eta_p^2 = .217$. Pointing towards the church was easier
 520 when coming from D1 (i.e., facing south; town hall: $M = 107.7^\circ \pm 31.5^\circ$; church: $M = 65.6^\circ \pm 36.0^\circ$) or D2 (i.e.,
 521 facing west; town hall: $M = 98.0^\circ \pm 39.4^\circ$; church: $M = 52.6^\circ \pm 40.8^\circ$), all $t \geq 3.19$, $p \leq .006$, $d \geq .773$. Finally, at I4,
 522 there was also an interaction between direction and target landmark, $F(3, 48) = 3.74$, $p = .017$, $\eta_p^2 = .190$.
 523 Performance was better when participants pointed towards the church ($M = 75.9^\circ \pm 30.8^\circ$) as compared to the
 524 town hall ($M = 106.6^\circ \pm 31.4^\circ$) when approaching the intersection from D2 (i.e., facing west), $t(16) = 2.59$, $p =$
 525 $.020$, $d = .629$.

526 To summarize, the results of this analysis again demonstrate better navigational encoding in younger
 527 adults and a higher reliance on the specific sensory input in older adults. The directions from which the older
 528 adults were approaching the intersections partly seemed to have an impact on their performance, although
 529 variability in performance was generally quite high.

530 Individual learning state and response time increase after direction change predict age-group

531 We next used a logistic regression model to check whether age-group can be determined based on two
 532 features that characterized age-related performance differences in our task. The mean amount of learning
 533 across the whole experiment (i.e., difference between individual learning state estimates from consecutive
 534 learning blocks) and the change in response times from the 4th to the 5th learning block served as input
 535 features. The model performed very well to estimate the probability of being classified as a younger adult with
 536 an average area under the curve (AUC) of $0.99 \pm 0.02\%$. Thus, those participants with a higher probability of

537 belonging to the younger age group show better performance on the task while a higher probability of being
 538 in the older age group relates to poorer navigational performance, i.e., a lower mean amount of learning
 539 across blocks and a higher increase in response times when previously learned locations are encountered from
 540 novel viewpoints (Figure 3D).

541 *fMRI experiment*

542 After pre-processing of the fMRI data using fmriprep (Esteban et al., 2019) and SPM12, we performed a
 543 univariate regression analysis to identify age-related differences in neural activity in the RSC/POS and the
 544 hippocampus during different phases of the experiment. We further examined the effects of learning at the
 545 within- and between-subject level. Finally, we examined age- and learning-related differences in effective
 546 connectivity within and between the two regions.

547 Learning ability varies within the older age group

548 As in the behavioral experiment, older compared to younger adults spent considerably more time in the initial
 549 familiarization phase of the experiment outside of the scanner ($M_{old} = 466 \text{ s} \pm 133 \text{ s}$; $M_{young} = 258 \text{ s} \pm 57.5 \text{ s}$;
 550 $t(44.3) = -7.91$, $p < .001$, $d = 2.03$). Moreover, we found significant main effects for learning block, $F(7, 385) =$
 551 32.3 , $p < .001$, $\eta_p^2 = .370$, and age group, $F(1, 55) = 167$, $p < .001$, $\eta_p^2 = .752$, together with a significant
 552 interaction between the two factors for the average absolute pointing errors, $F(7, 385) = 11.0$, $p < .001$, $\eta_p^2 =$
 553 $.166$. This indicates that younger compared to older adults again showed better performance on the task and
 554 stronger improvement across learning blocks (Figure 4A). Older adults, however, did show learning at the
 555 group level as confirmed by a separate ANOVA within this age group, $F(7, 217) = 3.58$, $p = .001$, $\eta_p^2 = .103$.
 556 Accuracy for the control trials was at ceiling across the whole sample (mean proportion of correct responses =
 557 0.97 ± 0.05). In contrast to the behavioral experiment, the change in directions from the first to the second half
 558 of the experiment was omitted here due to the reduced number of trials per learning block. Thus, we did not
 559 expect changes in response times from the first to the second half of the experiment.

560 Individual learning state estimates as obtained from the state-space model again showed that
 561 participants varied substantially in their ability to learn the spatial layout of the VE (Figure 4B, see also Figure
 562 3-1C-D for average pointing errors per learning block for each participant). To determine how neural activation
 563 patterns were modulated by the individuals' overall amount of learning across the experiment, we used a K-
 564 means clustering algorithm to identify learning sub-groups based on the difference between the latent state
 565 distributions of the last and first learning block. The estimated optimal number of clusters in our sample
 566 turned out to be five (Figure 4C): A group of *top learners* ($n = 9$), consisting of seven younger adults and two
 567 older adults, already learned the layout of the VE after the familiarization phase resulting in a small difference
 568 in learning between the first and the last learning block. The second cluster exclusively consisted of younger
 569 adults, categorized as *good learners* ($n = 14$). They typically reached ceiling performance during the first half of
 570 the experiment with a low variance in their difference distribution. A group of *intermediate learners* ($n = 9$),
 571 consisting of a three younger and six older adults, were still improving in the second half of the experiment
 572 and consequently exhibited the largest difference in their hidden learning state from the beginning to the end
 573 of the experiment and a relatively high variance. Individuals belonging to the fourth cluster were categorized
 574 as *weak learners* ($n = 12$) who showed only a small improvement across the whole experiment and a high

613

--- insert Figure 5 here ---

614 It is possible that the decreasing BOLD responses in the hippocampus and the increasing responses in
 615 RSC/POS, which we observed in younger adults, could have been driven by younger adults becoming quicker
 616 with self-localization, allowing them to compute the direction towards the target landmark at progressively
 617 earlier time points. Under this scenario, one would predict a temporal shift of the BOLD response, in particular
 618 for the RSC (assuming a role of the RSC/POS in deriving directional relationships between one's position and
 619 landmarks). To directly test this hypothesis, we performed a control analysis using a FIR model of the
 620 hemodynamic response but did not find any indications that the time bin of the peak of the HRF changed
 621 between the first and the second half of the experiment, neither in the hippocampus nor in the RSC/POS ROI.
 622 In the hippocampus, the median time bin was 3.75 (IQR = 1.25) in the first and 4.25 (IQR = 1.50) in the second
 623 half of the experiment in younger adults (out of 8 time bins that were modeled with a 2 s duration each). In
 624 older adults, the median in the first half was 4.50 (IQR = 1.44) and 4.50 (IQR = 0.75) in the second half. A two-
 625 sample Wilcoxon test confirmed that these differences were not significant in any of the experiment halves (all
 626 $p \geq .106$, Bonferroni corrected, all effect sizes $r \leq .262$). Similar results were obtained in the RSC/POS ROI with
 627 a median of 4.75 (IQR = 1.00) in the first and 4.50 (IQR = 1.00) in the second half within the younger age group
 628 and 4.50 (IQR = 1.19) in the first and 4.75 (IQR = 1.25) in the second half within the older age group (all $p \geq 1.00$,
 629 Bonferroni corrected, all effect sizes $r \leq .049$). This suggests that the differential hippocampal and RSC/POS
 630 dynamics in the two age groups are unlikely to be driven by changes in the onset/duration of the spatial
 631 computations carried out in the two regions.

632 Learning-related activity changes across blocks are modulated by inter-individual differences in learning
 633 within older adults

634 Behavioral performance of older adults varied substantially, with some of them showing hidden learning
 635 states similar to younger adults while others showed very little performance improvements. Therefore, we
 636 next included the individual's learning sub-group as covariate in the second-level analysis to examine in which
 637 regions learning-related activity changes across blocks differed as a function of the overall learning ability of
 638 the individual. In younger adults, no activations emerged within our ROIs or elsewhere in the brain. In older
 639 adults, however, we found that activity changes in several regions across the entire brain, including visual
 640 cortices, the cerebellum, temporal and frontal cortices, as well as the parahippocampal cortex (PHC)
 641 extending to the anterior hippocampus, were more strongly related to the individual learning curves in better
 642 performing groups (i.e., decreased across learning blocks, Figure 6, Figure 6-1). The learning curves of those
 643 older adults who were less able to learn the layout of the environment, in contrast, were decoupled from
 644 activity changes in these regions. No activations survived our correction for multiple comparisons within our
 645 ROIs or across the whole-brain when testing for the interactions between age group and learning sub-group.

646

--- insert Figure 6 here ---

647 Age-related reduction in the inhibitory self-connection of the anterior hippocampus

648 To check whether age-related problems in spatial learning are related to changes in the intrinsic excitability of
 649 the anterior hippocampus and the RSC/POS or in the coupling between the two regions, we used DCM PEB

650 (Friston et al., 2016). DCM has been successfully used to determine effective connectivity changes in the
 651 hippocampus and related regions during memory processing (Gluth et al., 2015). Moreover, DCM PEB offers
 652 several advantages over classical DCM variants in terms of model selection and second-level group
 653 comparisons. First, instead of specifying several models at the first level and comparing their evidence, a full
 654 model is estimated for each participant incorporating all parameters of interest, and Bayesian model
 655 reduction (BMR) is performed to obtain posterior estimates of nested models in which parameters that do not
 656 contribute to the model evidence are pruned. Second, first-level DCMs are equipped with empirical priors that
 657 shrink parameter estimates towards a group mean. In this way, each subject's contribution to the group PEB
 658 result is weighted by their precision. Third, applying classical inference methods to examine whether certain
 659 parameters differ between groups after model inversion ignores within-subject uncertainty (i.e., variance of
 660 the posterior distributions). This is circumvented in PEB by using the full posterior density over the parameters
 661 from each participant's DCM to draw inferences about group level effects.

662 For each participant, we first specified and estimated a DCM between the anterior hippocampus and
 663 the POS using peak coordinates from the corresponding univariate analysis. Navigational retrieval phases
 664 were modeled as driving input into the network via the POS. The amount of learning per block was modeled
 665 as modulatory input on the bidirectional connections between the two regions (Figure 7A). In the second-level
 666 PEB model, we included age group, learning sub-group, and their interaction as covariates to determine their
 667 relative influence on the connection strengths. The left panels in Figure 7 show the group mean of the average
 668 connection strength before (Figure 7B) and after BMR (Figure 7D), indicating that all four parameters were
 669 necessary to explain our data.

670 With respect to age group differences in connectivity, only one parameter survived BMR (second
 671 panels of Figure 7B and 7D). Specifically, older compared to younger adults had a reduced inhibitory self-
 672 connection strength in the anterior hippocampus, i.e., a relative disinhibition in this region. Note that for self-
 673 connections in the DCM framework, parameters are expressed as log scaling parameters and that the
 674 regressor representing age group was coded in a way that the resulting parameter is the amount that needs to
 675 be added to the group mean to obtain the older adults' connection strength (the group mean is obtained by
 676 calculating $-0.5\text{Hz} * \exp(-0.33698) = -0.357\text{Hz}$ and for older adults $-0.5\text{Hz} * \exp(-0.33698 + -0.039719) = -$
 677 0.3431Hz). Thus, our model provides evidence that the aging hippocampus seems to be more readily excited
 678 by afferent activity from other regions during spatial learning. The interaction between age group and
 679 learning sub-group in this model parameter also survived BMR (right panels in Figure 7B and 7D), indicating
 680 that the hippocampal self-connection strength was more strongly modulated by the overall learning ability of
 681 the individual in the older age group. Inspection of the fourth panel in Figure 7D indicates that the age-related
 682 disinhibition in this region was attenuated in better performing individuals (see also Figure 7C for posterior
 683 probabilities of each parameter). We did not find any modulatory effects of the (within-subject) amount of
 684 learning per block.

685 We further performed a leave-one-out (LOO) cross-validation using the model parameter denoting
 686 the self-connection strength in the anterior hippocampus to test whether this effect would be large enough to
 687 predict the participants' age group. In this analysis, all but one subject were used to estimate the model
 688 parameter, which was then used to evaluate the posterior belief of the model parameter in a left-out (test)

689 subject. The predicted and actual between-subject effect for each test subject was then compared to derive an
690 independent out-of-sample correlation, which was 0.29 in the current sample ($p=0.01434$, Figure 7E). Thus,
691 the estimated intrinsic connection strength in the anterior hippocampus during spatial learning was large
692 enough to predict the age group of a new subject above chance level.

693 *--- insert Figure 7 here ---*

694 **Summary of the key findings**

695 At the behavioral level, we found in two separate experiments that performance improvements were
696 considerably reduced in healthy older compared to younger adults, when they were asked to retrieve the
697 spatial layout of an initially unfamiliar environment. Older adults further showed a higher uncertainty when
698 familiar locations were experienced from novel viewpoints during learning, as evidenced by a temporary
699 increase in response times. At the neural level, activity in the anterior hippocampus and RSC/POS changed
700 dynamically as a function of learning in younger adults, whereas this was not the case in older adults.
701 Importantly, a DCM PEB analysis revealed that the inhibitory self-connection of the anterior hippocampus was
702 reduced in older adults and was modulated by the overall learning ability of the individual as evidenced by an
703 interaction between age group and learning sub-group (see Figure 8 for a graphical summary of the results).

704 *--- insert Figure 8 here ---*

705 **DISCUSSION**

706 In two experiments, we show that healthy older adults, on average, have substantial problems in learning to
707 orient themselves in a novel, city-like virtual environment, in line with previous findings (Iaria et al., 2009;
708 Yamamoto and DeGiolamo, 2012). At neural levels, we could replicate earlier findings showing that activity in
709 RSC/POS increased while activity in the anterior hippocampus decreased as a function of learning in younger
710 adults (Wolbers and Büchel, 2005; Auger et al., 2015; Brodt et al., 2016), which shows that our task is suitable
711 to measure spatial learning, while using a complex photorealistic VE. In older adults, activity in these two
712 regions was decoupled from the amount of learning and did not change systematically across repeated
713 episodes in the environment. Importantly, we provide the first evidence that an increased excitability of the
714 anterior hippocampus might constitute a potential neural mechanism for cognitive mapping deficits in older
715 adults.

716 In the behavioral experiment, we additionally found that older adults had problems when locations
717 are encountered from novel directions during learning. This might be related to age-related deficits in
718 distinguishing novel from familiar input (Yassa et al., 2011; Vieweg et al., 2015) and to impairments in
719 allocentric processing, because Wiener et al. (2013) observed age-related performance declines when
720 locations were approached from novel directions during route learning. Given that viewpoint transformations
721 in spatial memory involve hippocampal computations (King et al., 2002), the behavioral results already point
722 to impaired information processing within the aging hippocampus that affects navigational learning. This
723 extends findings showing that a reduced sensitivity to changes in the environment might be linked to age-

724 related impairments in object-location binding and spatial perspective taking (Muffato et al., 2019; Segen et
725 al., 2020).

726 In the fMRI experiment, performance relied on the knowledge about the relation between the
727 participant's own position and the position of the target landmarks, while the change in viewpoints was
728 omitted. What neural mechanisms can account for the cognitive mapping deficits in older adults? The
729 learning-related activity decrease in the anterior hippocampus of younger adults was absent in older adults,
730 leading to an overall hippocampal hyperactivity. Similar effects have been observed in studies investigating
731 age-related deficits in pattern separation (Yassa et al., 2011; Reagh et al., 2018), as well as in rodent and non-
732 human primate studies on age-related changes in spatial navigation (Wilson et al., 2005; Thomé et al., 2016).
733 By examining effective connectivity, we were able to show, for the first time, that an age-related reduction in
734 the inhibitory self-connection strength of the anterior hippocampus might constitute the underlying neural
735 mechanism for the elevated signal in this region. Within the context of DCM, self-connection parameters
736 capture, at a macroscopic level, condition specific changes in the excitatory-inhibitory balance (Friston et al.,
737 2017). Because effective connectivity as inferred using DCM for fMRI is typically polysynaptic, we cannot
738 determine which class of cells or synapses underlie these effects. In memory-impaired monkeys, increased
739 firing rates in CA3 place cells have been linked to a reduced number of GABAergic inhibitory interneurons
740 (Thomé et al., 2016). Whether this is similarly the case in humans and how this is related to AD pathogenesis
741 are important questions for future research (Bi et al., 2020).

742 The age effect on the hippocampal self-connection strength was modulated by the learning ability of
743 the individual, suggesting that an increased hippocampal excitability might impair the formation of spatial
744 knowledge. Specifically, aberrant activity in the hippocampus could have affected the spatial resolution of the
745 emerging cognitive maps in older adults, in line with findings showing that (i) hippocampal lesion patients and
746 healthy older adults are impaired in forming high-resolution spatial representations when navigating novel
747 environments (Kolarik et al., 2016; Kolarik et al., 2018; Nilakantan et al., 2018), and (ii) that reducing
748 hippocampal hyperactivity with an anti-epileptic drug that targets excitatory neurotransmission improves
749 memory performance in amnesic patients (Bakker et al., 2015; see also Koh et al., 2013; Robitsek et al., 2015
750 for related findings in rodents). Critically, in the context of our task, imprecise cognitive maps will not only
751 affect self-localization but also the ability to compute allocentric vectors to the target landmarks. The latter
752 process has also been linked to computations in sub-regions of the MTL (Chadwick et al., 2015; Shine et al.,
753 2019; see also Wang et al., 2018; Høydal Ø et al., 2019).

754 In addition to hippocampal hyperactivation, older adults also exhibited a lack of learning related
755 dynamics in RSC/POS. Medial parietal cortex undergoes significant changes during aging, including increased
756 atrophy and enhanced tau deposition (Jockwitz et al., 2017; Harrison et al., 2019). Moreover, the increased
757 excitability of the aging hippocampus may impact on information processing in RSC/POS, given the close
758 reciprocal interactions between both regions. For example, Mao et al. (2018) found that bilateral hippocampal
759 lesions suppress the gradual emergence of a spatial code in the RSC. In the present study, given that RSC/POS
760 is assumed to support the anchoring of cognitive maps to external landmarks (Epstein et al., 2017), a deficient
761 anchoring may compromise older adults' ability to precisely recover their facing direction and to orient their
762 cognitive maps when approaching the intersections. Together with the imprecision in the cognitive maps,

763 both deficits are likely to contribute to the compromised pointing performance in older adults.

764 Moreover, this anchoring process should occur in parallel to self-localization in our task, because as
765 soon as an intersection was visible during navigational retrieval, participants could use the local buildings
766 and/or the geometric layout to recover both their position and their facing direction. This could explain why –
767 particularly in younger adults – the latency of the BOLD response in RSC/POS did not change over the course
768 of the experiment, because the process of reorientation could start immediately at the beginning of a trial.

769 Our univariate results differ from Moffat et al. (2006) who measured brain activity during encoding of
770 a virtual maze and reported an age-related hypoactivation in the RSC and the hippocampus. This discrepancy
771 might be related to the timepoint when activity was measured, because if younger adults were still acquiring
772 knowledge about the VE, our findings would also predict stronger hippocampal effects compared to older
773 adults. More generally, this discrepancy highlights the need to track the learning status of an individual when
774 interpreting differences in (hippocampal) BOLD responses between groups. In addition, it is important to note
775 that we focused on hemodynamic changes during retrieval in our study. Thus, overall task demands could be
776 another factor that might have contributed to our findings, because we also observed an age-related activity
777 increase in RSC/POS and hippocampus when contrasting retrieval to encoding.

778 Performance in our task was highly variable. While some older adults learned the layout of the
779 environment as quickly as younger adults, others showed continuous learning, learned very slowly, or were
780 not able to retrieve relevant information to perform the task. During MRI scanning, the amount of exposure in
781 the VE was kept constant for all participants. This allowed us to replicate earlier findings in younger adults and
782 to use this as a baseline against which we could compare the results of the older adults. Therefore, we cannot
783 determine whether low-performing older adults would just need more time for learning. However, it seems
784 unlikely that all of them would have reached the same performance level as younger adults if provided with
785 more time in the VE, because older adults already spent considerably more time in the initial familiarization
786 phase of the experiments. Using machine learning methods on MRI data of hundreds of older adults, Eavani et
787 al. (2018) described multiple phenotypes of brain agers that are characterized by specific functional and
788 structural changes. The authors described one phenotype that displays atrophy in the hippocampus,
789 decreased coherence in posterior medial parietal cortex, and an increased connectivity in the MTL. Thus, older
790 adults who show an increased excitability of the anterior hippocampus might be particularly impaired in
791 memorizing novel spatial environments.

792 Finally, by forming sub-groups of learners based on their estimated learning states and by including
793 this information in the fMRI analysis, we found that activity changes in several brain regions were decoupled
794 from the individual learning curves in those older adults who had more problems to learn. Although these
795 results should be interpreted with caution given the small sample sizes of our groups, they provide further
796 indications that hyperactivity in the aging brain does not seem to support task performance (Morcom and
797 Henson, 2018). We did not find any indications that the learning differences within older adults were related to
798 their age, sex, or their cognitive screening scores. Thus, future studies should apply additional measures, for
799 example preclinical markers for AD, to further characterize age-related deficits in spatial learning and,
800 specifically, why these abilities are preserved in some older adults.

801 Taken together, increased excitability of the anterior hippocampus, together with aberrant RSC/POS
802 functioning, provides a novel explanation why older adults experience problems with forming accurate spatial
803 representations of a novel environment. In addition, our findings add to a growing body of evidence
804 associating hyperactivity in the hippocampus to memory impairments in aging.

805 **REFERENCES**

- 806 Auger SD, Zeidman P, Maguire EA (2015) A central role for the retrosplenial cortex in de novo environmental
807 learning. *eLife* 4:e09031. doi: 10.7554/eLife.09031
- 808 Bakker A, Albert MS, Krauss G, Speck CL, Gallagher M (2015) Response of the medial temporal lobe network
809 in amnesic mild cognitive impairment to therapeutic intervention assessed by fMRI and memory task
810 performance. *NeuroImage: Clinical* 7:688-698.
- 811 Barnes CA, Suster MS, Shen J, McNaughton BL (1997) Multistability of cognitive maps in the hippocampus of
812 old rats. *Nature* 388:272-275.
- 813 Behzadi Y, Restom K, Liao J, Liu TT (2007) A component based noise correction method (CompCor) for BOLD
814 and perfusion based fMRI. *Neuroimage* 37:90-101.
- 815 Berens P (2009) CircStat: A MATLAB toolbox for circular statistics. *J Stat Softw* 31:1-21.
- 816 Bi D, Wen L, Wu Z, Shen Y (2020) GABAergic dysfunction in excitatory and inhibitory (E/I) imbalance drives the
817 pathogenesis of Alzheimer's disease. *Alzheimer's & Dementia* 16:1312-1329.
- 818 Braak H, Del Tredici K (2015) The preclinical phase of the pathological process underlying sporadic Alzheimer's
819 disease. *Brain* 138:2814-2833.
- 820 Brett M, Anton J-L, Valabregue R, Poline JB (2002) Region of interest analysis using an SPM toolbox.
821 *Neuroimage* 16.
- 822 Brodt S, Pöhlchen D, Flanagan VL, Glasauer S, Gais S, Schönauer M (2016) Rapid and independent memory
823 formation in the parietal cortex. *Proc Natl Acad Sci USA* 113:13251-13256.
- 824 Bzdok D, Heeger A, Langner R, Laird AR, Fox PT, Palomero-Gallagher N, Vogt BA, Zilles K, Eickhoff SB (2015)
825 Subspecialization in the human posterior medial cortex. *Neuroimage* 106:55-71.
- 826 Carpenter B, Gelman A, Hoffman MD, Lee D, Goodrich B, Betancourt M, Brubaker M, Guo J, Li P, Riddell A
827 (2017) Stan: A probabilistic programming language. *J Stat Softw* 76:1-32.
- 828 Chadwick MJ, Jolly AEJ, Amos DP, Hassabis D, Spiers HJ (2015) A goal direction signal in the human
829 entorhinal/subicular region. *Curr Biol* 25:87-92.
- 830 Commandeur J, Koopman SJ (2007) Introduction to state space time series analysis. Oxford: Oxford University
831 Press.
- 832 Dale AM, Fischl B, Sereno MI (1999) Cortical surface-based analysis: I. Segmentation and surface
833 reconstruction. *Neuroimage* 9:179-194.
- 834 Daunizeau J, Stephan KE, Friston KJ (2012) Stochastic dynamic causal modelling of fMRI data: Should we care
835 about neural noise? *Neuroimage* 62:464-481.
- 836 Destrieux C, Fischl B, Dale AM, Hagren E (2010) Automatic parcellation of human cortical gyri and sulci using
837 standard anatomical nomenclature. *Neuroimage* 53:1-15.
- 838 Diersch N, Wolbers T (2019) The potential of virtual reality for spatial navigation research across the adult
839 lifespan. *The Journal of Experimental Biology* 222. doi: 10.1242/jeb.187252
- 840 Eavani H, Habes M, Satterthwaite TD, An Y, Hsieh M-K, Honnorat N, Erus G, Doshi J, Ferrucci L, Beason-Held
841 LL, Resnick SM, Davatzikos C (2018) Heterogeneity of structural and functional imaging patterns of advanced
842 brain aging revealed via machine learning methods. *Neurobiol Aging* 71:41-50.
- 843 Epstein RA (2008) Parahippocampal and retrosplenial contributions to human spatial navigation. *Trends Cogn
844 Sci* 12:388-396.

- 845 Epstein RA, Patai EZ, Julian JB, Spiers HJ (2017) The cognitive map in humans: Spatial navigation and beyond.
846 *Nat Neurosci* 20:1504-1513.
- 847 Esteban O, Birman D, Schaer M, Koyejo OO, Poldrack RA, Gorgolewski KJ (2017) MRIQC: Advancing the
848 automatic prediction of image quality in MRI from unseen sites. *PLOS ONE* 12:e0184661. doi:
849 10.1371/journal.pone.0184661
- 850 Esteban O, Markiewicz C, Blair RW, Moodie C, Isik AI, Erramuzpe Aliaga A, Kent J, Goncalves M, DuPre E,
851 Snyder M, Oya H, Ghosh SS, Wright JD, Durnez J, Poldrack RA, Gorgolewski KJ (2019) FMRIPrep: A robust
852 preprocessing pipeline for functional MRI. *Nature Methods* 16:111-116.
- 853 Faul F, Erdfelder E, Lang A-G, Buchner A (2007) G*Power 3: A flexible statistical power analysis program for
854 the social, behavioral, and biomedical sciences. *Behavior Research Methods* 39:175-191.
- 855 Fischl B, Sereno MI, Dale AM (1999) Cortical surface-based analysis: II: Inflation, flattening, and a surface-
856 based coordinate system. *Neuroimage* 9:195-207.
- 857 Fischl B, Salat DH, Busa E, Albert M, Dieterich M, Haselgrove C, van der Kouwe A, Killiany R, Kennedy D,
858 Klaveness S, Montillo A, Makris N, Rosen BR, Dale AM (2002) Whole brain segmentation: Automated labeling
859 of neuroanatomical structures in the human brain. *Neuron* 33:341-355.
- 860 Friston KJ, Preller KH, Mathys C, Cagnan H, Heinzle J, Razi A, Zeidman P (2017) Dynamic causal modelling
861 revisited. *Neuroimage*. doi: 10.1016/j.neuroimage.2017.02.045
- 862 Friston KJ, Litvak V, Oswal A, Razi A, Stephan KE, van Wijk BCM, Ziegler G, Zeidman P (2016) Bayesian model
863 reduction and empirical Bayes for group (DCM) studies. *Neuroimage* 128:413-431.
- 864 Gelman A, Shirley K (2011) Inference from simulations and monitoring convergence. In: *Handbook of Markov*
865 *Chain Monte Carlo* (Brooks S, Gelman A, Jones GL, Meng X-L, eds), pp 163-174. Boca Raton, FL: Chapman
866 Hall.
- 867 Gluth S, Sommer T, Rieskamp J, Büchel C (2015) Effective connectivity between Hippocampus and
868 ventromedial Prefrontal Cortex controls preferential choices from memory. *Neuron* 86:1078-1090.
- 869 Gorgolewski KJ et al. (2016) The brain imaging data structure, a format for organizing and describing outputs
870 of neuroimaging experiments. *Scientific Data* 3:160044. doi: 10.1038/sdata.2016.44
- 871 Grady CL (2012) The cognitive neuroscience of ageing. *Nat Rev Neurosci* 13:491-505.
- 872 Grinband J, Steffener J, Razlighi QR, Stern Y (2017) BOLD neurovascular coupling does not change
873 significantly with normal aging. *Hum Brain Mapp* 38:3538-3551.
- 874 Harrison TM, La Joie R, Maass A, Baker SL, Swinnerton K, Fenton L, Mellinger TJ, Edwards L, Pham J, Miller
875 BL, Rabinovici GD, Jagust WJ (2019) Longitudinal tau accumulation and atrophy in aging and alzheimer
876 disease. *Ann Neurol* 85:229-240.
- 877 Høydal Ø A, Skytøen ER, Andersson SO, Moser MB, Moser EI (2019) Object-vector coding in the medial
878 entorhinal cortex. *Nature* 568:400-404.
- 879 Iaria G, Palermo L, Committeri G, Barton JJS (2009) Age differences in the formation and use of cognitive
880 maps. *Behav Brain Res* 196:187-191.
- 881 Jockwitz C, Caspers S, Lux S, Jütten K, Schleicher A, Eickhoff SB, Amunts K, Zilles K (2017) Age- and function-
882 related regional changes in cortical folding of the default mode network in older adults. *Brain Struct Funct*
883 222:83-99.
- 884 Jones E, Oliphant T, Peterson P (2001) SciPy: Open source scientific tools for Python. In. <http://www.scipy.org>.

- 885 King JA, Burgess N, Hartley T, Vargha-Khadem F, O'Keefe J (2002) Human hippocampus and viewpoint
886 dependence in spatial memory. *Hippocampus* 12:811-820.
- 887 Kobayashi Y, Amaral DG (2003) Macaque monkey retrosplenial cortex: II. Cortical afferents. *The Journal of*
888 *Comparative Neurology* 466:48-79.
- 889 Koh MT, Rosenzweig-Lipson S, Gallagher M (2013) Selective GABAA α 5 positive allosteric modulators
890 improve cognitive function in aged rats with memory impairment. *Neuropharmacology* 64:145-152.
- 891 Kolarik BS, Baer T, Shahlaie K, Yonelinas AP, Ekstrom AD (2018) Close but no cigar: Spatial precision deficits
892 following medial temporal lobe lesions provide novel insight into theoretical models of navigation and
893 memory. *Hippocampus* 28:31-41.
- 894 Kolarik BS, Shahlaie K, Hassan AS, Borders AA, Kaufman KC, Gurkoff G, Yonelinas AP, Ekstrom AD (2016)
895 Impairments in precision, rather than spatial strategy, characterize performance on the virtual Morris Water
896 Maze: A case study. *Neuropsychologia* 80:90-101.
- 897 Konishi K, Etchamendy N, Roy S, Marighetto A, Rajah N, Bohbot VD (2013) Decreased functional magnetic
898 resonance imaging activity in the hippocampus in favor of the caudate nucleus in older adults tested in a
899 virtual navigation task. *Hippocampus* 23:1005-1014.
- 900 Leal SL, Landau SM, Bell RK, Jagust WJ (2017) Hippocampal activation is associated with longitudinal amyloid
901 accumulation and cognitive decline. *eLife* 6:e22978. doi: 10.7554/eLife.22978
- 902 Lester AW, Moffat SD, Wiener JM, Barnes CA, Wolbers T (2017) The aging navigational system. *Neuron*
903 95:1019-1035.
- 904 Li B, Daunizeau J, Stephan KE, Penny WD, Hu D, Friston K (2011) Generalised filtering and stochastic DCM for
905 fMRI. *Neuroimage* 58:442-457.
- 906 Luis CA, Keegan AP, Mullan M (2009) Cross validation of the Montreal Cognitive Assessment in community
907 dwelling older adults residing in the Southeastern US. *Int J Geriatr Psychiatry* 24:197-201.
- 908 Mao D, Neumann AR, Sun J, Bonin V, Mohajerani MH, McNaughton BL (2018) Hippocampus-dependent
909 emergence of spatial sequence coding in retrosplenial cortex. *Proc Natl Acad Sci USA*. doi:
910 10.1073/pnas.1803224115
- 911 Miller AMP, Vedder LC, Law LM, Smith DM (2014) Cues, context, and long-term memory: The role of the
912 retrosplenial cortex in spatial cognition. *Front Hum Neurosci* 8:1-15. doi: 10.3389/fnhum.2014.00586
- 913 Moffat SD, Elkins W, Resnick SM (2006) Age differences in the neural systems supporting human allocentric
914 spatial navigation. *Neurobiol Aging* 27:965-972.
- 915 Morcom AM, Henson RNA (2018) Increased Prefrontal activity with aging reflects nonspecific neural responses
916 rather than compensation. *J Neurosci* 38:7303-7313.
- 917 Muffato V, Hilton C, Meneghetti C, De Beni R, Wiener JM (2019) Evidence for age-related deficits in object-
918 location binding during place recognition. *Hippocampus* 29:971-979.
- 919 Nasreddine ZS, Phillips NA, Bédirian V, Charbonneau S, Whitehead V, Collin I, Cummings JL, Chertkow H
920 (2005) The Montreal Cognitive Assessment, MoCA: A brief screening tool for mild cognitive impairment. *J Am*
921 *Geriatr Soc* 53:695-699.
- 922 Nilakantan AS, Bridge DJ, VanHaerents S, Voss JL (2018) Distinguishing the precision of spatial recollection
923 from its success: Evidence from healthy aging and unilateral mesial temporal lobe resection.
924 *Neuropsychologia* 119:101-106.

- 925 Oldfield RC (1971) The assessment and analysis of handedness: The Edinburgh inventory. *Neuropsychologia*
926 9:97-113.
- 927 Patai EZ, Javadi A-H, Ozubko JD, O'Callaghan A, Ji S, Robin J, Grady C, Winocur G, Rosenbaum RS,
928 Moscovitch M, Spiers HJ (2019) Hippocampal and Retrosplenial goal distance coding after long-term
929 consolidation of a real-world environment. *Cereb Cortex*. doi: 10.1093/cercor/bhzo44
- 930 Pedregosa F, Varoquaux G, Gramfort A, Michel V, Thirion B, Grisel O, Blondel M, Prettenhofer P, Weiss R,
931 Dubourg V, Vanderplas J, Passos A, Cournapeau D, Brucher M, Perrot M, Duchesnay E (2011) Scikit-learn:
932 Machine learning in python. *J Mach Learn Res* 12:2825-2830.
- 933 Poppenk J, Evensmoen HR, Moscovitch M, Nadel L (2013) Long-axis specialization of the human
934 hippocampus. *Trends Cogn Sci* 17:230-240.
- 935 Reagh ZM, Noche JA, Tustison NJ, Delisle D, Murray EA, Yassa MA (2018) Functional imbalance of
936 anterolateral entorhinal cortex and hippocampal dentate/CA3 underlies age-related object pattern separation
937 deficits. *Neuron* 97:1187-1198.
- 938 Robitsek J, Ratner MH, Stewart T, Eichenbaum H, Farb DH (2015) Combined administration of levetiracetam
939 and valproic acid attenuates age-related hyperactivity of CA3 place cells, reduces place field area, and
940 increases spatial information content in aged rat hippocampus. *Hippocampus* 25:1541-1555.
- 941 Rosenbaum RS, Winocur G, Binns MA, Moscovitch M (2012) Remote spatial memory in aging: all is not lost.
942 *Front Ag Neurosci* 4:1-10. doi: 10.3389/fnagi.2012.00025
- 943 Rugg MD, Morcom AM (2005) The relationship between brain activity, cognitive performance and aging: The
944 case of memory. In: *Cognitive neuroscience of aging: Linking cognitive and cerebral aging* (Cabeza R, Nyberg
945 L, Park DC, eds), pp 132-154. New York, NY: Oxford University Press.
- 946 Segen V, Avraamides MN, Slattery TJ, Wiener JM (2020) Age-related differences in visual encoding and
947 response strategies contribute to spatial memory deficits. *PsyArXiv*. doi: 10.31234/osf.io/4qdey
- 948 Shine JP, Valdés-Herrera JP, Tempelmann C, Wolbers T (2019) Evidence for allocentric boundary and goal
949 direction information in the human entorhinal cortex and subiculum. *Nature Communications* 10:4004. doi:
950 10.1038/s41467-019-11802-9
- 951 Smith AC, Wirth S, Suzuki WA, Brown EN (2007) Bayesian analysis of interleaved learning and response bias in
952 behavioral experiments. *J Neurophysiol* 97:2516-2524.
- 953 Stan Development Team (2017) PyStan: the Python interface to Stan. In, 2.16.0.0. Edition. <http://mc-stan.org>.
- 954 Thomé A, Gray DT, Erickson CA, Lipa P, Barnes CA (2016) Memory impairment in aged primates is associated
955 with region-specific network dysfunction. *Mol Psychiatry* 21:1257.
- 956 Vehtari A, Gelman A, Gabry J (2017) Practical Bayesian model evaluation using leave-one-out cross-validation
957 and WAIC. *Statistics and Computing* 27:1413-1432.
- 958 Vieweg P, Stangl M, Howard LR, Wolbers T (2015) Changes in pattern completion – A key mechanism to
959 explain age-related recognition memory deficits? *Cortex* 64:343-351.
- 960 Wang C, Chen X, Lee H, Deshmukh SS, Yoganarasimha D, Savelli F, Knierim JJ (2018) Egocentric coding of
961 external items in the lateral entorhinal cortex. *Science* 362:945-949.
- 962 Wiener JM, de Condappa O, Harris MA, Wolbers T (2013) Maladaptive bias for extrahippocampal navigation
963 strategies in aging humans. *J Neurosci* 33:6012-6017.
- 964 Wilson IA, Ikonen S, Gallagher M, Eichenbaum H, Tanila H (2005) Age-associated alterations of hippocampal
965 place cells are subregion specific. *J Neurosci* 25:6877-6886.

- 966 Wolbers T, Büchel C (2005) Dissociable Retrosplenial and Hippocampal contributions to successful formation
967 of survey representations. *J Neurosci* 25:3333-3340.
- 968 Yamamoto N, DeGirolamo G (2012) Differential effects of aging on spatial learning through exploratory
969 navigation and map reading. *Front Ag Neurosci* 4:1-7. doi: 10.3389/fnagi.2012.00014
- 970 Yassa MA, Lacy JW, Stark SM, Albert MS, Gallagher M, Stark CEL (2011) Pattern separation deficits associated
971 with increased hippocampal CA3 and dentate gyrus activity in nondemented older adults. *Hippocampus*
972 21:968-979.
- 973 Zeidman P, Maguire EA (2016) Anterior hippocampus: The anatomy of perception, imagination and episodic
974 memory. *Nat Rev Neurosci* 17:173-182.
- 975 Zeidman P, Jafarian A, Seghier ML, Litvak V, Cagnan H, Price CJ, Friston KJ (2019a) A guide to group effective
976 connectivity analysis, part 2: Second level analysis with PEB. *Neuroimage* 200:12-25.
- 977 Zeidman P, Jafarian A, Corbin N, Seghier ML, Razi A, Price CJ, Friston KJ (2019b) A guide to group effective
978 connectivity analysis, part 1: First level analysis with DCM for fMRI. *Neuroimage*. doi:
979 10.1016/j.neuroimage.2019.06.031

980 **FIGURE LEGENDS**981 **Figure 1.** Spatial learning task.

982 (A) Procedure of the fMRI experiment. After a familiarization phase outside of the scanner, eight retrieval
 983 phases, each comprising 8 navigational retrieval trials and 4 control trials, alternated with 7 encoding phases
 984 during scanning. In the behavioral experiment, the structure was the same except that 12 navigational
 985 retrieval trials per learning block were completed while the control trials were omitted. (B) Layout of the
 986 virtual environment (VE). The VE resembled a typical German historic city center and consisted of four
 987 interconnected intersections (I1-I4) that could be reached from 4 directions (D1-D4). At two intersections, a
 988 town hall (T1) and a church (T2) were placed at the end of one of the outgoing streets that served as target
 989 landmarks in the navigational retrieval trials. Yellow arrows exemplify one encoding tour that started from
 990 one of the target landmarks in clockwise or counterclockwise direction (a short segment of one tour is shown
 991 in Video 1). (C) Structure of one example navigational retrieval trial to measure spatial learning. After fixation,
 992 participants were passively transported towards one of four intersections in the VE starting from one of the
 993 four streets leading towards that intersection (see Video 2). Movement stopped at the center of the
 994 intersection, a red crosshair appeared, and participants were asked to move the crosshair in the direction of
 995 the respective target landmark. During the entire duration of the trial, a picture cue of the target landmark
 996 was displayed at the bottom of the screen, and the background was obscured by fog to prevent seeing the
 997 target landmarks. In the fMRI experiment, an additional jittered interval of 1 s (still phase) was added after the
 998 travel phase/before the crosshair appeared on screen.

999 **Figure 2.** Bayesian state-space model to estimate the subject-specific hidden learning state per learning block
 1000 (see Figure 2-1 for the model code). Results of the posterior predictive checks of the model for representative
 1001 individuals from each learning sub-group in the fMRI experiment and a histogram of the individuals' loo
 1002 differences for the comparison of the Bayesian state-space model to an alternative model that estimated the
 1003 individuals' learning state trial-wise is depicted in Figure 2-2.

1004 **Figure 3.** Performance data in the behavioral experiment.

1005 (A) Average absolute pointing errors and (B) response times across the eight learning blocks in older (solid
 1006 line) and younger adults (dashed line; highlighted in grey is the 4th and 5th learning block where the change in
 1007 directions took place from which the intersections were approached). Error bars denote standard errors of the
 1008 means (SE). See also Figure 3-1A-B for average pointing errors per learning block for each participant in each
 1009 age group. (C) Mean estimated performance improvement (hidden learning state) of each participant in the
 1010 older (orange) and younger (grey) age group, including the standard deviation (SD) of the posterior
 1011 distributions (shaded area) across learning blocks. (D) Logistic regression results classifying age group
 1012 membership based on two behavioral performance features, i.e., the mean amount of learning across the
 1013 experiment and the increase in response times after the first half of the experiment. Shaded lines depict the
 1014 probability of being classified as a younger adult.

1015 **Figure 4.** Performance data in the fMRI experiment.

1016 (A) Average absolute pointing errors across the eight learning blocks in older (solid line) and younger adults
 1017 (dashed line). Error bars denote standard errors of the means (SE). See also Figure 3-1C-D for average pointing
 1018 errors per learning block for each participant in each age group. (B) Mean estimated performance
 1019 improvement (hidden learning state) of each participant in the older (orange) and younger (grey) age group,
 1020 including the standard deviation (SD) of the posterior distributions (shaded area) across learning blocks. (C)
 1021 Learning sub-groups as identified by a K-means clustering algorithm based on the individuals' overall amount
 1022 of learning and its SD, as determined by the difference of the latent state distributions of the last and first
 1023 learning block. See Figure 4-1 for difference distributions, learning state estimates, and performance data per
 1024 learning block for representative individuals from each learning sub-group and Figure 4-2 for the results of the
 1025 same clustering analysis within the sample of the behavioral experiment.

1026 **Figure 5.** Interaction effects between age group and the amount of learning per block during navigational
 1027 retrieval. Age-related differences in (A) hippocampal activity decreases and (B) RSC/POS activity increases
 1028 across the experiment. Activations are displayed on the 2009 nonlinear asymmetric MNI template that was
 1029 used for normalization ($p < 0.05$, FWE-corrected for the respective ROI). Plots depict average parameter
 1030 estimates of the respective peak voxels per learning block in selected clusters for each age group. Error bars
 1031 indicate the across-subject standard error of the mean. See Table 1 for the spatial coordinates of the local
 1032 maxima in the hippocampus and RSC/POS ROIs and Table 1-1 for significantly activated clusters elsewhere in
 1033 the brain.

1034 **Figure 6.** Differential activity changes in relation to the amount of learning per block between learning sub-
 1035 groups in the older age group. Activations are displayed on the 2009 nonlinear asymmetric MNI template that
 1036 was used for normalization ($p < 0.05$, FWE-corrected). See Figure 6-1 for the spatial coordinates of the local
 1037 maxima.

1038 **Figure 7.** Results of the DCM PEB analysis. (A) First-level DCM specification to determine average connectivity
 1039 within and between anterior hippocampus and POS. Navigational retrieval phases were modeled as driving
 1040 input entering the cortical network via the POS, and the amount of learning per block was included as
 1041 modulatory input on the bidirectional connections between the regions. Estimated Parameters (1: self-
 1042 connection POS, 2: POS – hippocampus connection, 3: hippocampus – POS connection, 4: self-connection
 1043 hippocampus) (B) before and (D) after Bayesian model reduction (BMR) for each covariate (age group,
 1044 learning group, interaction between age group and learning group) in the second-level PEB model. Grey bars
 1045 represent parameter means and pink lines their 95% confidence intervals. The parameters for self-connections
 1046 (parameter 1 and 4) are expressed as log scaling parameters that can be converted to Hz using $x_{\text{Hz}} = -0.5 * \exp(x)$
 1047 whereby x is the log scaling parameter and -0.5 Hz the prior. (C) Posterior probabilities per parameter
 1048 for each second-level covariate after BMR, (E) Predicted age group of each participant as derived from a LOO
 1049 cross-validation scheme based on the estimated self-connection strength in the anterior hippocampus.

1050 **Figure 8.** Key findings of the two experiments.

1051 **Video 1.** Exemplary segment of one of the tours through the virtual environment in the encoding phases of
 1052 the two experiments.

1053 **Video 2.** Example for a pointing trial in the retrieval phases of the two experiments.

1054 **TABLES**

1055 **Table 1.** Spatial coordinates of the local maxima in the hippocampus and RSC/POS ROIs in the fMRI analyses
 1056 on age-related differences in neural activation patterns ($p < 0.05$, FWE-corr.). See Table 1-1 for significantly
 1057 activated clusters elsewhere in the brain.

Brain region	Cluster size	MNI coordinate			Z-score
		x	y	z	
A) Increased activity in older compared to younger adults during navigation vs. control					
L POS	83	-3	-60	34	4.56
L RSC		-6	-57	21	4.32
L Hippocampus	72	-21	-18	-12	4.76
		-30	-15	-22	4.21
B) Reduced activity in older compared to younger adults during navigation vs. control					
R POS	22	12	-69	54	4.00
		18	-69	57	3.94
		15	-75	51	3.25
R POS	55	27	-60	24	3.96
C) Increased activity in older compared to younger adults during retrieval vs. encoding					
R POS	27	12	-51	34	4.03
L Hippocampus	33	-30	-15	-15	4.08
R Hippocampus	20	24	-12	-12	3.97
D) Age-group differences in learning-related activity decreases					
R Hippocampus	20	24	-18	-15	4.55
E) Age-group differences in learning-related activity increases					
L POS	462	-9	-66	24	5.93
		-24	-72	47	5.37
L RSC		-18	-57	1	4.14
		-6	-63	11	3.98
R POS	148	24	-69	47	4.95
		21	-72	54	4.73
R RSC	205	9	-57	4	4.82
		9	-63	21	4.59

1058

1 **TABLE AND FIGURE LEGENDS**

2 **Table 1-1, related to Table 1 and Figure 5:** Spatial coordinates of the local maxima in the whole-brain fMRI analyses on
 3 age-related differences in neural activation patterns ($p < 0.05$, whole-brain FWE-corr.).

4 **Figure 2-1, related to Figure 2 and Bayesian Modeling of Performance Data section:** Stan code of the Bayesian state-
 5 space model.

6 **Figure 2-2, related to Figure 2 and Bayesian Modeling of Performance Data section:** Results of the posterior predictive
 7 checks of the Bayesian state-space model for representative individuals from each learning sub-group (A: top learner
 8 young – E: non-learner old; see Performance Clustering section; the posterior predictive samples distribution, y_{repr} , plotted
 9 together with the observed data points, y , per learning block) and (F) histogram of the individuals' loo differences for the
 10 comparison of the Bayesian state-space model incorporating the effects of the responses, η , to an alternative model that
 11 estimated the individuals' learning state trial-wise. More positive values indicate a better fit of the first model.

12 **Figure 3-1, related to Figure 3 and 4:** Average absolute pointing errors per learning block for each participant in (A) the
 13 younger and (B) the older age group in the behavioral experiment, and for each participant in (C) the younger and (D) the
 14 older age group in the fMRI experiment.

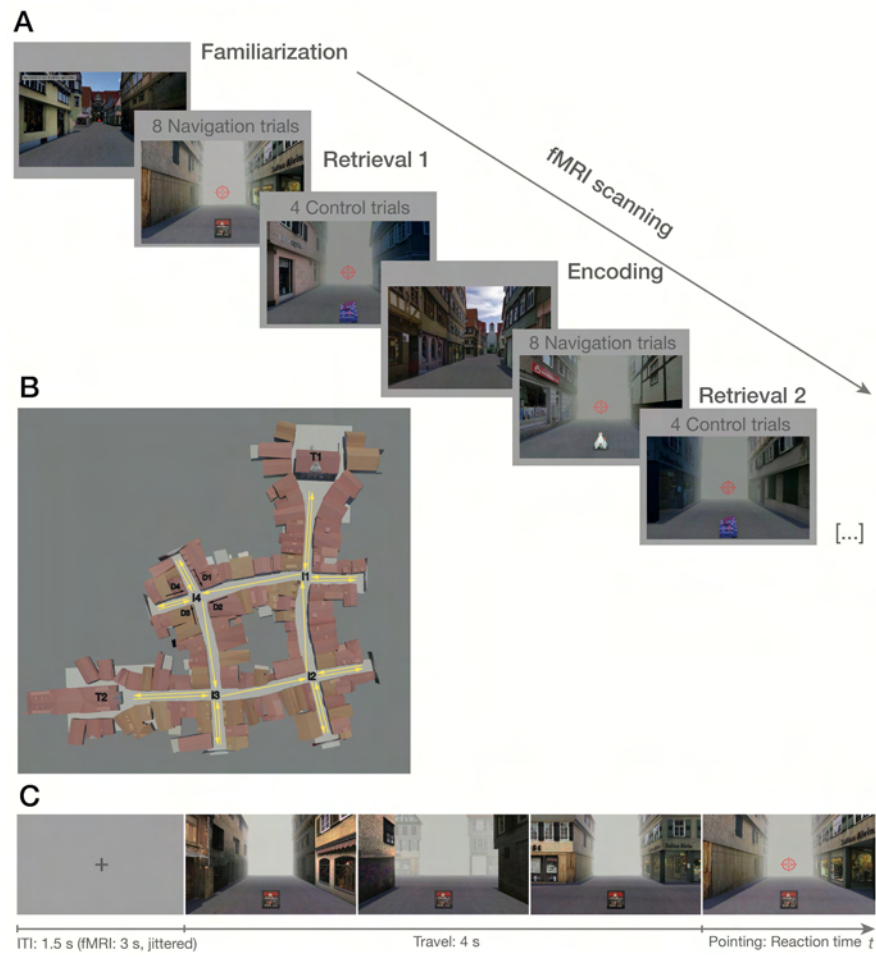
15 **Figure 4-1, related to Figure 4 and Performance Clustering section:** Definition of learning sub-groups. Hidden learning
 16 states (including SD) and trial-wise performance data per learning block (left) and the latent state distributions of the last
 17 and first learning block plotted together with the difference distribution (right) from representative individuals from each
 18 learning sub-group in the fMRI experiment.

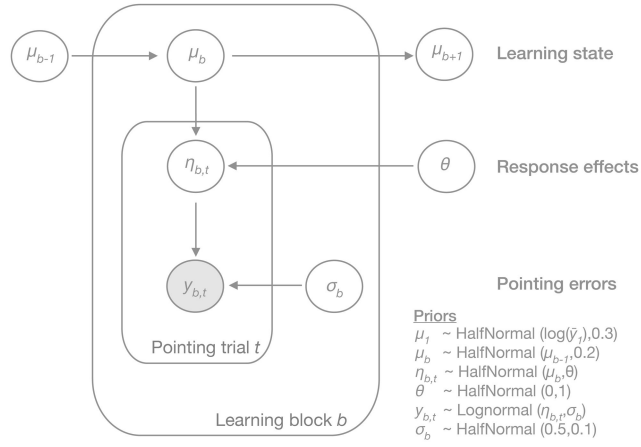
19 **Figure 4-2, related to Figure 4 and Performance Clustering section:** Learning sub-groups in the behavioral experiment as
 20 identified by a K-means clustering algorithm based on the individuals' overall amount of learning and its SD, as
 21 determined by the difference of the latent state distributions of the last and first learning block. Results are shown for (A) 5
 22 and (B) 6 learning clusters that yielded similar silhouette scores (respective mean silhouette scores per tested cluster
 23 number: 3: 0.232, 4: 0.293, 5: 0.400, 6: 0.404, 7: 0.370).

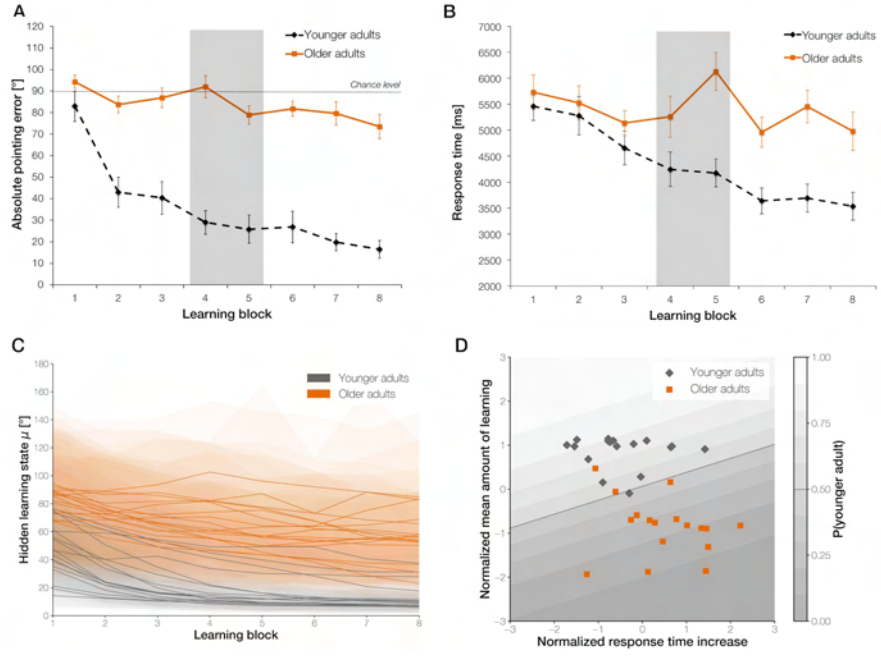
24 **Figure 4-3, related to Figure 4 and Performance Clustering section:** Key demographics of the learning sub-groups within
 25 each age group in the fMRI experiment.

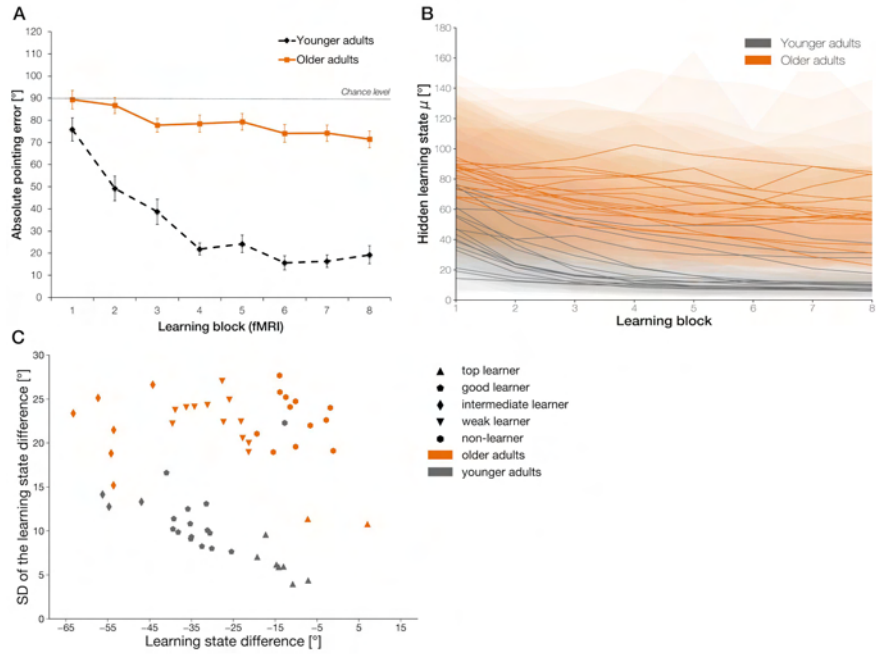
26 **Figure 5-1, related to Figure 5 and Table 1:** Spatial coordinates of the local maxima in the whole-brain fMRI analyses on
 27 age-related differences in neural activation patterns ($p < 0.05$, whole-brain FWE-corr.).

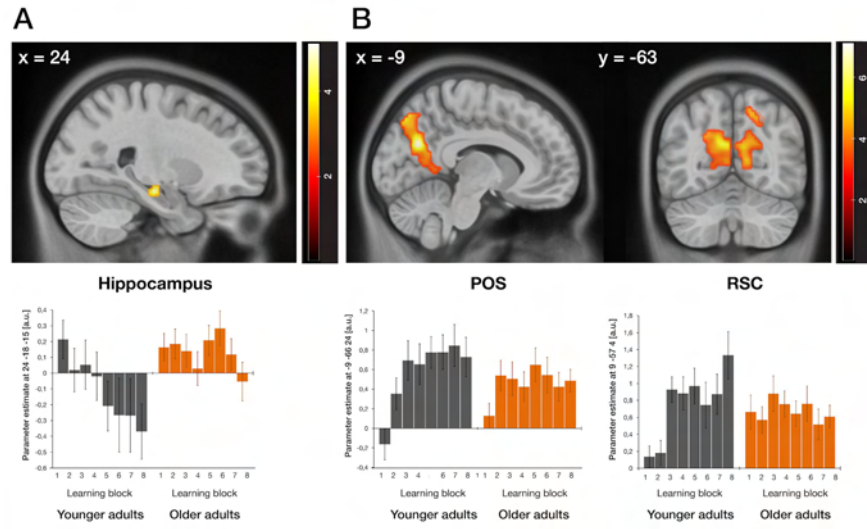
28 **Figure 6-1, related to Figure 6:** Spatial coordinates of the local maxima in the fMRI analyses on inter-individual
 29 differences in neural activation patterns across learning blocks within older adults ($p < 0.05$, FWE-corr.).
 30

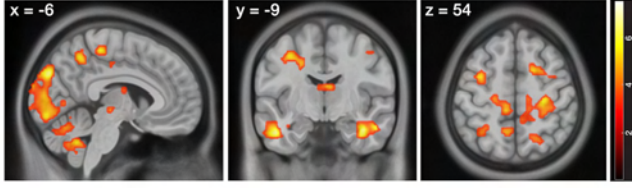


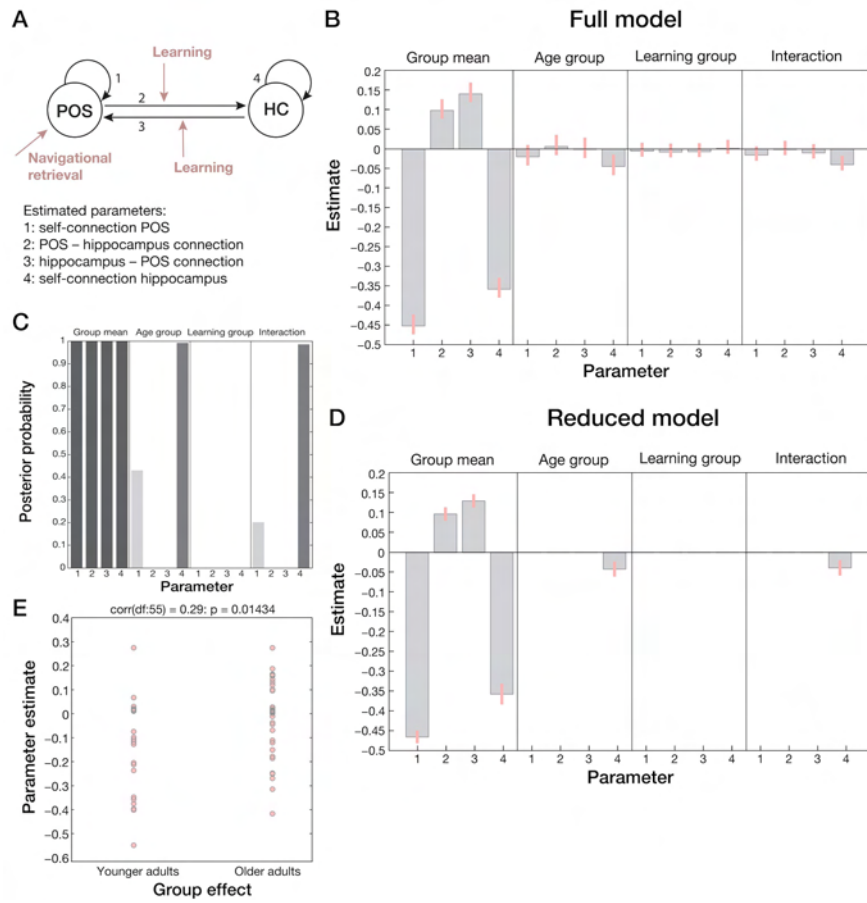












Key findings

